

## Optimization of a Frame of Stair-Climbing Wheelchair Structure by Using GREY-TOPSIS



Duc Tin Do<sup>ID</sup>, Ngoc Dong Nguyen<sup>ID</sup>, Quoc An Tran<sup>ID</sup>, Nhat Quang Nguyen<sup>ID</sup>, Ngoc Thai Huynh<sup>\*ID</sup>

Faculty of Mechanical Engineering Technology, Ho Chi Minh City University of Industry and Trade, Ho Chi Minh 700000, Vietnam

Corresponding Author Email: [thaihn@huit.edu.vn](mailto:thaihn@huit.edu.vn)

Copyright: ©2024 The authors. This article is published by IETA and is licensed under the CC BY 4.0 license (<http://creativecommons.org/licenses/by/4.0/>).

<https://doi.org/10.18280/mmep.111214>

### ABSTRACT

**Received:** 28 August 2024

**Revised:** 17 October 2024

**Accepted:** 25 October 2024

**Available online:** 31 December 2024

#### Keywords:

*stair-climbing wheelchair, grey relational analysis, TOPSIS method, finite element analysis, MERE method*

Designing and manufacturing a wheelchair is a very simple task. A wheelchair that can move on uneven roads, such as climbing stairs, is not simple. This problem is a big challenge for researchers. In this study, the wheelchair model is designed to help the elderly, disabled people, and people unable to walk more conveniently. 27 climbing upstairs vehicle models were designed by using Inventor software. Durability analysis of the vehicle body structure during motion is performed using Transient structural analysis in ANSYS. The strain and stresses of the vehicle body are optimized using grey relational analysis and TOPSIS methods. The results of Transient structural analysis in ANSYS indicated that the selected dimension of cross-section of the bar of the frame of climbing upstairs vehicle greatly affect the strain and stress of the vehicle body. The optimal results of the grey relational analysis method and the TOPSIS method also confirm this. The predicted and optimal values of strain and stress were 0.000436 mm and 85.756 MPa, respectively. The error percentage between the predicted and optimal values of strain and stress were very low not exceeding 0.68% and 2.14%, respectively. The optimal results shown that the vehicle moves stably up the stairs while still ensuring the durability of the wheelchair under the condition Vehicle weight is about 60kg, passenger weight is about 50kg. While the wheelchair moves in the x direction at 100t mm (t is time), the wheelchair moves in the y direction at 20 + 50t mm, the wheelchair axis rotates around the z axis at an angle of 40t degrees.

## 1. INTRODUCTION

Nowadays, the need to use electric wheelchairs as a means of transportation for the elderly or after an accident is increasing. Electric wheelchairs meet several essential needs, including mobility: Electric wheelchairs allow users to move independently without the assistance of others. This helps them fully participate in daily activities, such as work, school, and social activities. Electric wheelchairs are easy to use and control, even for people with limited strength or mobility. They can also navigate a variety of terrain, helping users reach more places. Electric wheelchairs give users a feeling of independence and autonomy. They no longer have to depend on others for transportation, which can have huge benefits for their mental and physical health. Electric wheelchairs help users access areas and activities that they may not be able to access without a vehicle. This includes public buildings, public transportation, and even some types of outdoor terrain. Electric wheelchairs are designed to be safe and stable, even when used on rough terrain. They can also be equipped with safety features such as seat belts and indicator lights. Improved quality of life: Electric wheelchairs can help users significantly improve their overall quality of life by increasing mobility, independence, and access. Overall, an electric wheelchair is an essential tool that meets a number of essential needs for people with disabilities. They provide mobility,

convenience, independence, accessibility and safety, helping users live more fulfilling and active lives. There are many researchers around the world who design and manufacture wheelchairs for climbing stairs. To ensure stability when climbing stairs, optimal design parameters were selected using the Taguchi method [1]. The improved rocker-bogie system not only prevents instability caused by the robot's wheels tipping over, but also increases the ability to climb stairs. A structure designed to transport goods over uneven surfaces such as stairs [2]. Different materials were also tested to select an even model that was both durable and lightweight. Simulation analysis results using SolidWorks software indicated that aluminum alloy is not only light but also has high durability. To reduce the weight of the device to assist people with difficulty walking, especially when moving up stairs, the WeMo Structure [3] was proposed. To climb stairs easily, it is necessary to have a device to detect stairs and locate the structure of the stairs, 2D LiDAR [4]. The K-Means and RANSAC algorithm was applied to determine the riser height and tread depth of stairs. The rocker bogie [5] designed for rough terrain has improved mechanical strength, structural soundness, stability. The axle transfer wheel mechanism is designed for stair climbing wheelchairs to reduce slopes [6]. The results of mathematical analysis have been verified experimentally. The triple interlocking wheel wheelchair is a design for transporting goods upstairs [7]. The design achieved

a cargo transport efficiency of 87%. The opening of the wheel foot in Clause 1.1 to 1.53 [8] ensures the wheelchair climbed up the stairs. Design method using wheels with a simulation. The stair climbing performance of the wheelchair is achieved based on the transport capacity index, maximum cross slope and maximum climbing speed [9]. The six-wheeled rover stair-climbing wheelchair maintains vehicle stability when climbing stairs thanks to the stair positioning model [10]. The results pointed out that this model achieves a stair positioning efficiency of up to 99.64%. Stair climbing performance based on proposed sensing method [11]. The results were also compared with several other stair wheelchairs. A 6-legged automatic stair climbing robot is controlled by Q-Whex [12]. Experimental results identified that the proposed model achieves high performance, the vehicle is stable when going up stairs and on uneven roads. 6-degree-of-freedom robotic arm integrated with tracked chassis, sensors and controller [13]. The vehicle overcomes obstacles with its unique rotating arm and is stable when climbing stairs. In addition, the robot arm also has depth camera support and LIDAR support base. AnyBody 7.2 human model [14] is used to simulate the kinematics and dynamics of the joints of the stair climbing wheelchair. Joint forces and moments and stresses are simulated by using ANSYS. The finite element analysis results have confirmed that the stair climbing wheelchair is always in a stable state. A bionic OCV compound [15] can cope with rough terrain and uneven roads such as stairs integrated into the wheelchair to easily move people or objects or help rescue after an accident effectively. The kinematic and dynamic states of the stair climbing robot are analyzed based on the analysis of the changes in the position of the center of gravity, the angle and the maximum width of the robot body when climbing stairs [16]. The results of this analysis are the basis for easier robot control. Leg robots [17] are an effective solution for any terrain including stairs. Test results pointed out that 4-legged robots move effectively when going up stairs. The self-adaptive deformable chain mechanism [18] is designed to overcome rough terrain especially upstairs and downstairs. Experimental results demonstrate effective terrain overcoming. The proposed mechanism can move forward and backward flexibly. Variable diameter wheels are designed to cope with obstacles [19] or when climbing slopes or stairs. Experiments have shown that variable diameter wheels ensure effective control when climbing slopes or stairs. The gripper is designed to grasp and climb stairs, and a set of rails to move on flat roads [20]. These two sets are designed for a military robot to climb stairs. To make the robot climb stairs easily, sensors are also integrated to detect stairs and measure the height and slope of the stairs. Experiments show that the design is very effective in climbing stairs. The design of the chain wheel structure and the change of the seat angle for the wheelchair help the wheelchair climb stairs easily, reducing the cost of buying a new wheelchair [21]. Reduce jerking for wheelchairs when going up stairs, by using B-spline [22]. The steering torque and jerk values were significantly reduced by 9.5% and 92%, respectively. The humanoid robot NANO [23] is designed to climb down stairs. The robot's horizontal walking is established through the inverted pendulum model. The vision system is applied to detect stairs. The Webots platform is applied to simulate robot movement. Experimental results show that the robot's gait is highly effective when climbing stairs. Robots that support walking or help pick up things from remote locations [24] are divided into 5 types: wheeled type, crawler type, climbing leg structure type, mixed

wheel and track type. Simple operation, low maintenance costs, high safety index. A crawler stair climbing robot [25] has been designed and manufactured. The dynamics of the stair-climbing robot were analyzed using MATLAB Simulink and validated using ADAMS Tracked Vehicle software. The tail mechanism designed for a three-wheeled stair-climbing robot [26] moves more stably and is also confirmed by experiments.

The main goal of the project is to optimally design and manufacture an automatic stair-climbing wheelchair model to help the elderly, disabled, sick or people with difficulty walking or accidents. Easy to move up and down stairs. Optimum design of stair access mechanism for wheelchairs with maximum load capacity of 50 kg, ensuring wheelchair durability using grey relational analysis optimization method and TOPSIS method [27] based on the results of finite element analysis in ANSYS. Design an automatic controller for easy and convenient loading and unloading of the vehicle. Design and optimize analysis of electric wheelchairs for the elderly and disabled using a model built on INVENTOR software based on collected documents and an overview of documents on vehicle structure. rolling, moving method, material, operating method. Durability analysis and dynamic analysis for wheelchairs using ANSYS software. Selecting the optimal model for manufacturing using optimization algorithms Grey relational analysis based on the Taguchi method and TOPSIS method. Design new and improved electric wheelchairs, including off-road electric wheelchairs and stair-climbing electric wheelchairs. Develop new materials and technologies to make electric wheelchairs lighter, more durable and more efficient. Improve the automation of electric wheelchairs to make them more comfortable and easier to use for users.

Previous studies focused on establishing the differential equation of motion of the stair climbing wheelchair and analyzing the static strength of the vehicle frame. In this study, the stress and strain of vehicle frame and blocking devices were analyzed while moving up the stairs. Transient simulation of 27 cases analysis was performed based on the design results of the Taguchi method through MiniTab software to analyze the influence of design dimensions on the relative stress and deformation of the wheelchair when climbing stairs, then applying the grey relational analysis method to confirm the results of finite element analysis and select the optimal solution. These results were also compared with the multi-criteria decision-making method TOPSIS method. The optimal cases of these two methods were confirmed by Taguchi method (signal to noise analysis), Mean value analysis, interaction analysis, variance analysis, statistical analysis, 3D surface graph analysis. Finally, the Taguchi method also compared the forecast results and the optimal results.

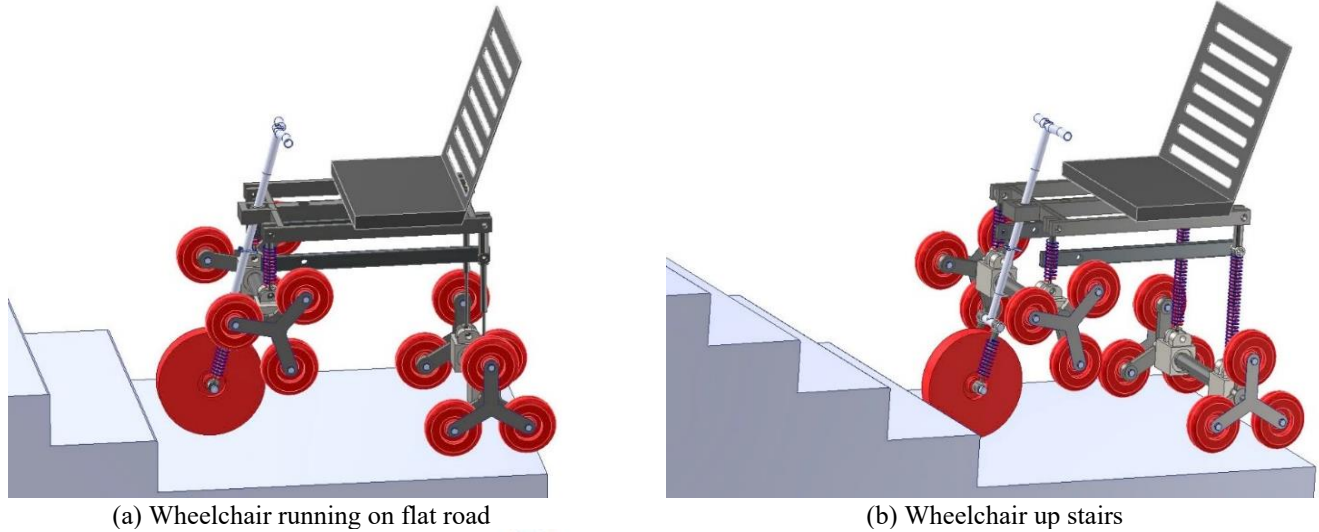
## **2. STAIR CLIMBING WHEELCHAIR MODEL DESIGN AND FINITE ELEMENT ANALYSIS**

### **2.1 Design 3D model**

The model is designed on the Inventor platform as shown in Figure 1. The car body model includes assembled details such as: Seat, frame, 160 mm×50 mm wheels, axle, sturdy bars, details to install axle, stiffener bar for chassis, 135 mm fork, 335 mm fork, details to install wheels, engine, chain transmission, bearings, stairs. The vehicle uses 3 wheels to go

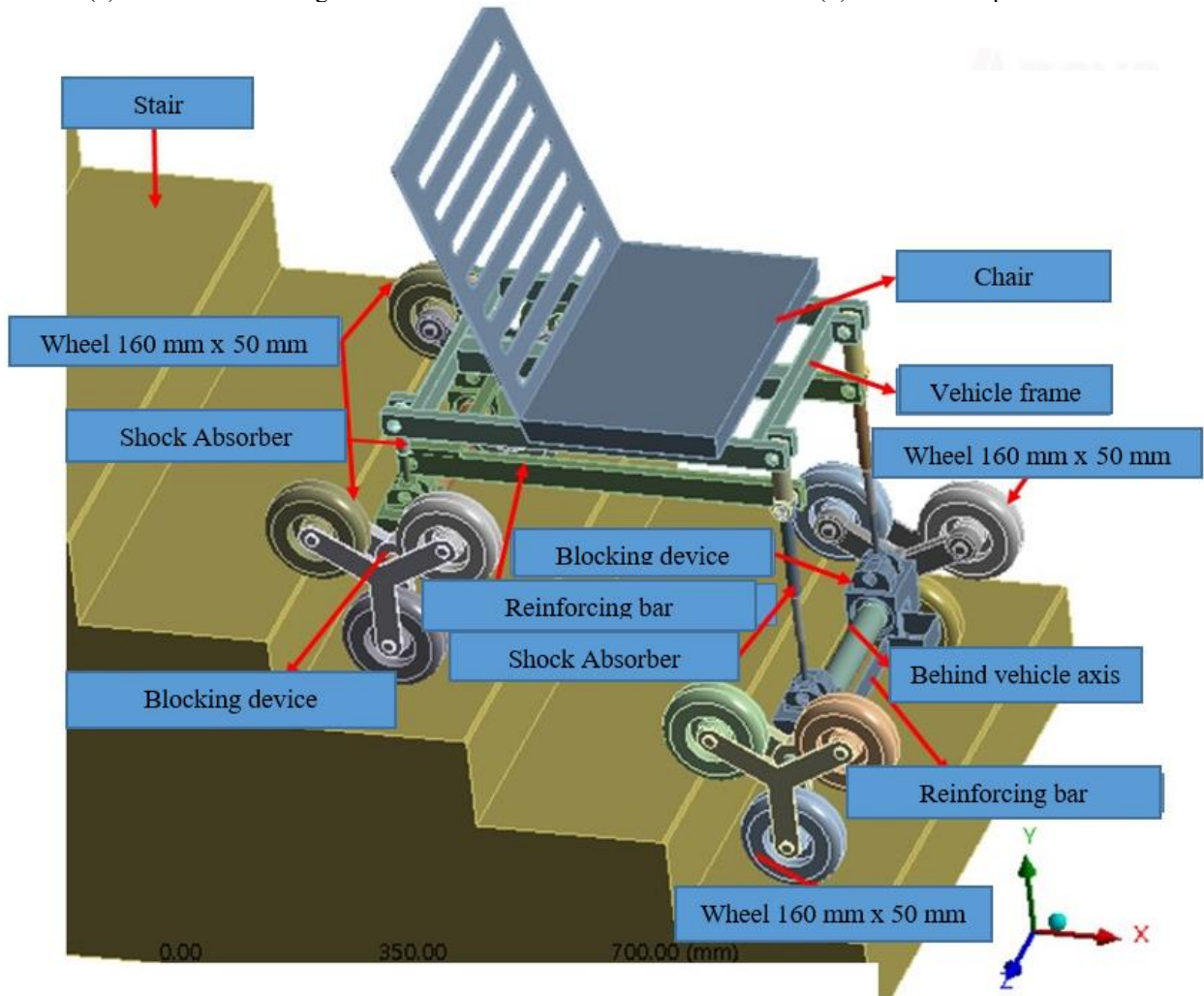
up the stairs, driven from the motor with 600w-12VDC-3.9 kg to the front axle of the vehicle through the chain transmission and then to the rear axle of the vehicle thanks to the chain transmission, turning the rotational motion of the engine into translational motion for vehicle. The 3 wheels are distributed at an angle of 120°, allowing the car to go up the stairs easily. To ensure that the vehicle can still run on flat roads, a large wheel of having 300 mm diameter is also designed to be

installed in the front of the frame as presented in Figure 1(a). When going up the stairs, this wheel is pulled up to avoid this wheel hitting the stairs as presented in Figure 1(b) obstructing access to stairs. When reaching the last step or when going down the last step, the middle wheel will fold down so that the car can run on a flat road normally. The overall dimensions of the vehicle and the weight of the vehicle are 900 mm×600 mm×700 mm and 50 kg respectively.



(a) Wheelchair running on flat road

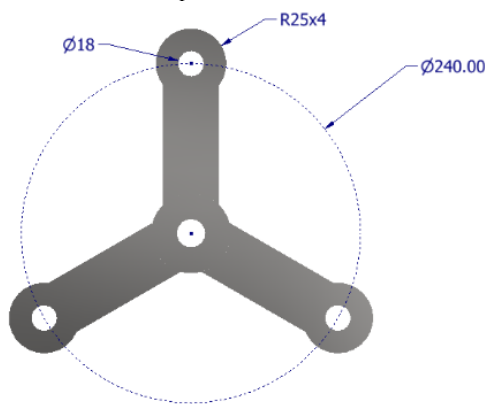
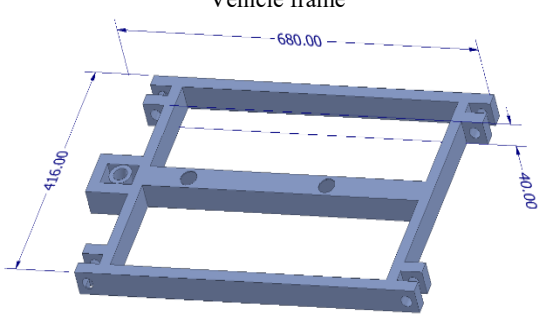
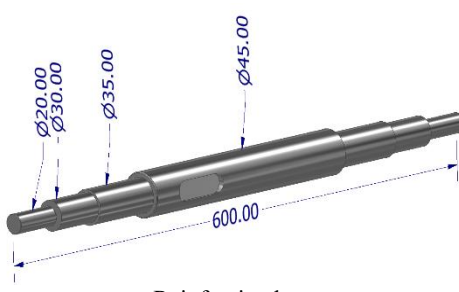

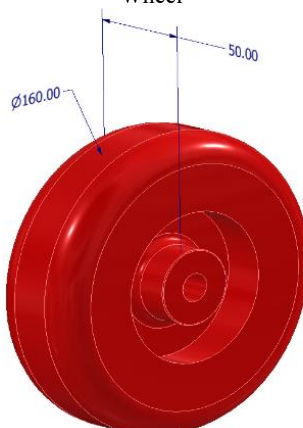
(b) Wheelchair up stairs


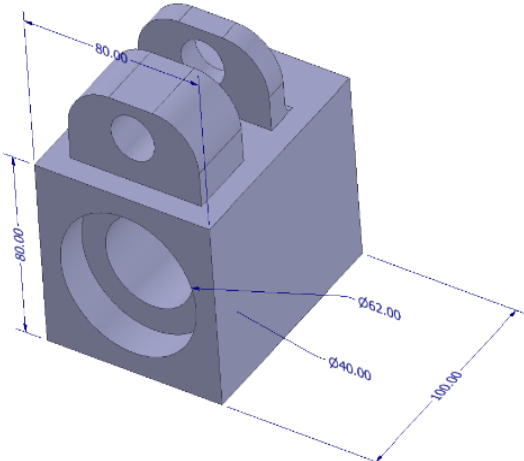



(c) Wheelchair model for simulation

Figure 1. Wheelchair up stairs

**Table 1.** Material properties of the part

Part No.	Name's part	Material	Young's Modulus	Poisson Ratio
	Blocking device Made of ss304 square stainless steel 20 mm×35 mm×1.4 mm			
1	 <p>Vehicle frame</p>	SS304	210 GPa	0.3
	 <p>Front and Behind vehicle axis</p>	SS304	210 Gpa	0.3
2	 <p>Reinforcing bar</p>	SS304	210 GPa	0.3
3		SS304	210 GPa	0.3
4	 <p>Wheel</p>	rubber	0.1 Mpa	0.4

Part No.	Name's part	Material	Young's Modulus	Poisson Ratio
5	Shock Absorber Length of the rear shock absorber is 235 mm  Length of the front of shock absorber is 13 mm.	Structural steel	210 GPa	0.3
6	Bearing socket 	Structural steel	210 GPa	0.3
7	Ball bearing 	Chrome Steel - SAE 52100	210 GPa	0.3

## 2.2 Simulation setup in ANSYS transient structural

To simplify the simulation process, the chain transmission is not included in the simulation model. First, the wheelchair models up the stairs is put into the Transient structural environment in ANSYS as shown in Figure 2. Declare materials for the model. In this study, the vehicle frame material and wheel mounting details were chosen as Inox SS304 rectangular steel with a cross section of 20 mm×40 mm×1.4 mm. The elastic modulus of this material is 210 GPa, Poisson's coefficient is 0.3 as listed in Table 1. To ensure the durability of the wheelchair when going up stairs as well as when moving on the ground, these two details need to ensure durability. Therefore, it is necessary to analyze the stress and strain for these two details. The remaining details are considered absolutely solid. Next create connection joints for the model including fixed ground joints to fix the rod bridge, fixed joints, and revolute joints and translation joints to connect the details for connection. The fork's motion is

modeled using springs and dampers with spring stiffness of 500 N/m and 500 Ns/mm. Load the model as follows: the person sitting in the wheelchair is modeled as a concentrated force acting on the vehicle frame of 500 N equivalent to 50kg. The vehicle's motion as presented in Eq. (1) is set using the Remote displacement tool as shown in Figure 2.

$$\begin{cases} x = 100t \text{ (mm)} \\ y = 50t + 20 \text{ (mm)} \\ z = 40t \text{ (degrees)} \end{cases} \quad (1)$$

where,  $t$  is the simulation time set to 9 seconds.

The results of this simulation are the stress and strain of the vehicle frame, axle mounting details, dynamic joint pressure acting on the vehicle axle... However, this study only considers the stress and strain of the vehicle frame and mounting details. wheels because these two parts bear the most force when the vehicle moves.



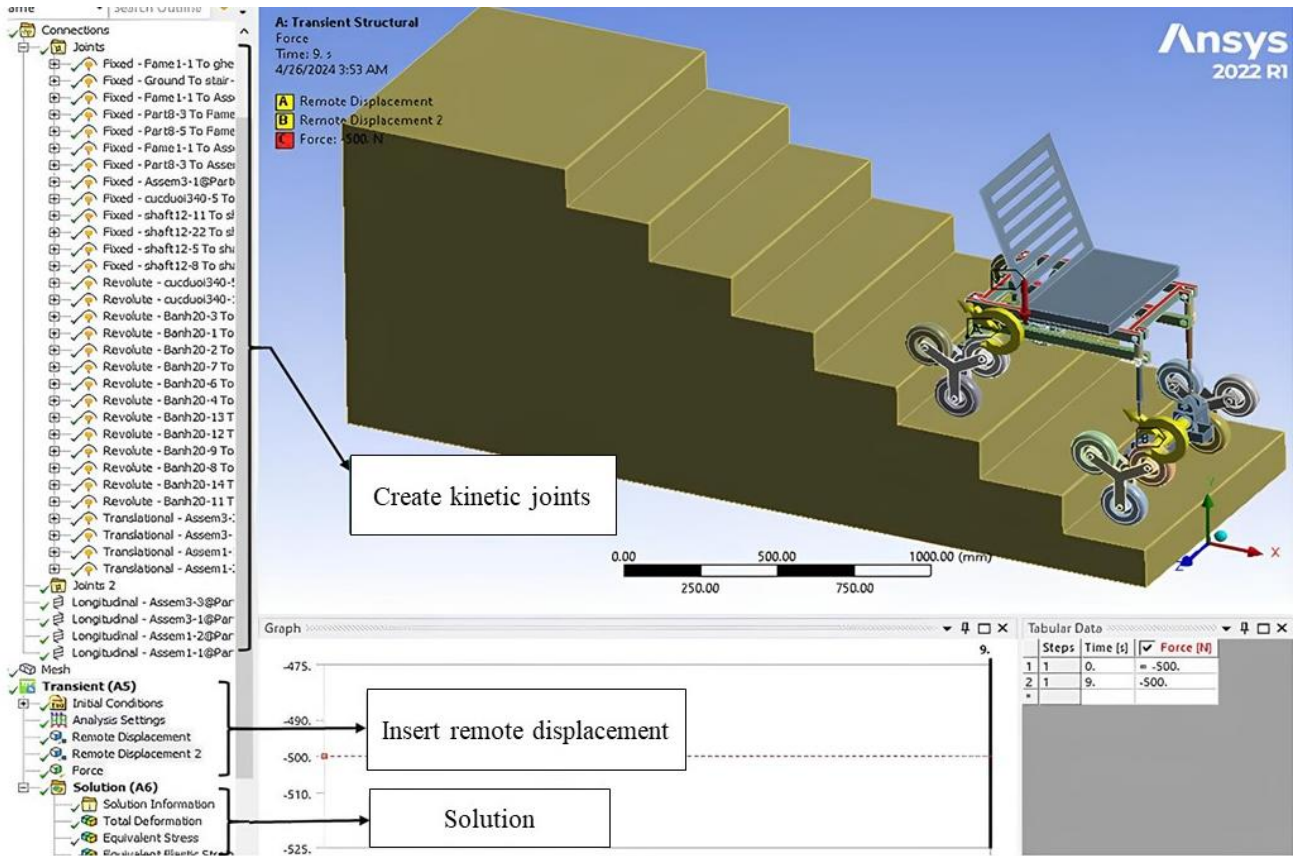


Figure 2. Simulation setup in transient structural

### 3. OPTIMAL METHOD

#### 3.1 MEREC weight determination method

MEREC method [28-30] used to calculate weights for the above methods are presented in the following steps:

Step 1: Calculate the normalized values according to the following equations:

The criteria of the objective were determined.

If the objective is the bigger is the better:

$$h_{ij} = \frac{\min u_{ij}}{u_{ij}} \quad (2)$$

If the objective is the smaller is the better:

$$h_{ij} = \frac{u_{ij}}{\max u_{ij}} \quad (3)$$

where,  $u_{ij}$  is the output value. In this investigation,  $u_{ij}$  represents the values of the strain and stress, which were obtained from transient dynamic in ANSYS.

Step 2: Total performance of the criteria was determined.

$$S_i = \ln \left[ 1 + \left( \frac{1}{n} \sum_j |\ln(h_{ij})| \right) \right] \quad (4)$$

Step 3: The performance of the criteria was determined.

$$S'_{ij} = \ln \left[ 1 + \left( \frac{1}{n} \sum_{k, k \neq j} |\ln(h_{ij})| \right) \right] \quad (5)$$

Step 4: The deviation was determined:

$$E_j = |S'_{ij} - S_i| \quad (6)$$

Step 5: The weight of every criterion was determined.

$$w_j = \frac{E_j}{\sum_k E_k} \quad (7)$$

#### 3.2 Grey relational analysis

The optimization process is used using MiniTab 20 software to create orthogonal arrays, the optimal output characteristics are achieved as the theoretical model must first indicate, and then the optimization methods are applied.

Step 1: Select combination parameters that optimize output characteristics.

Step 2: Design control elements and their levels.

Step 3: Arrange orthogonal array L27 using MiniTab.

Step 4: Conduct simulation and collect simulation data.

Optimization steps using grey relational analysis GRA [31-37], to optimize these output characteristics.

Grey relational analysis (GRA) is a method of comparing changes in a system under analysis to estimate the importance of design variables. GRA was applied to separate the sequences. GRA is performed as follows:

Normalize: Rewrite each string from 0 to 1 as follows:

The larger the objective is the better was determined as following:

$$D_i^* = \frac{D_i^{(0)}(k) - \min D_i^0(k)}{\max D_i^{(0)}(k) - \min D_i^0(k)} \quad (8)$$

The smaller the objective is the better was determined as following:

$$D_i^* = \frac{\max D_i^{(0)}(k) - D_i^0(k)}{\max D_i^{(0)}(k) - \min D_i^0(k)} \quad (9)$$

Grey coefficient (GRC) represents the distance between the standard value under consideration and the ideal value. Determining GRC is required before determining grey relationship level (GRG). Deviation calculation formula:

$$\Delta_{0i} = \|D_0^*(k) - D_i^*(k)\| \quad (10)$$

$$\Delta_{\min} = \max_{\forall j \in i} \min_{\forall k} \|D_0^*(k) - D_j^*(k)\| \quad (11)$$

$$\Delta_{\max} = \max_{\forall j \in i} \max_{\forall k} \|D_0^*(k) - D_j^*(k)\| \quad (12)$$

Formula to calculate grey relationship coefficient (GRC):

$$\gamma_i(k) = \frac{\Delta_{\min} + \xi \Delta_{\max}}{\Delta_{0i} + \xi \Delta_{\max}} \quad (13)$$

where,  $\Delta_{0i}$  is the absolute value of the deviation between the standard value and the ideal value  $\xi \in [0,1]$  is usually taken as 0.5.

GRG grey level ( $\Psi_i$ ) is determined as follows:

$$\Psi_i = \sum_{k=1}^n \omega_k \gamma_i(k) \quad (14)$$

where,  $n$  is the number of experiments.

### 3.3 Method (TOPSIS)

The steps to analyze simulation results using TOPSIS [38-41] are applied as follows:

Step 1: Build an evaluation matrix.

$$X = [x_{ij}]_{m \times n} = \begin{bmatrix} x_{11} & \cdot & \cdot & \cdot & x_{1n} \\ x_{21} & \cdot & \cdot & \cdot & x_{2n} \\ \cdot & \cdot & \cdot & \cdot & \cdot \\ \cdot & \cdot & \cdot & \cdot & \cdot \\ \cdot & \cdot & \cdot & \cdot & \cdot \\ x_{m1} & \cdot & \cdot & \cdot & x_{mn} \end{bmatrix} \quad (15)$$

where,  $m$  is the number of options,  $n$  is the number of criteria,  $x$  is the value of criterion  $j$  in option  $i$ .

Step 2: Standardize research data.

$$K_{ij} = \frac{x_{ij}}{\sqrt{\sum_{i=1}^m x_{ij}^2}} \quad (16)$$

Step 3: Calculate the weighted average:

$$W_{ij} = w_j \times K_{ij} \quad (17)$$

Step 4: Calculate the positive optimal fuzzy solution ( $A^+$ ) and the negative optimal fuzzy solution ( $A^-$ ) are calculated according to the formula:

$$A^+ = \{k_1^+, k_2^+, \dots, k_j^+, \dots, k_n^+\} \quad (18)$$

$$A^- = \{k_1^-, k_2^-, \dots, k_j^-, \dots, k_n^-\} \quad (19)$$

where,  $k_j^+$  and  $k_j^-$  are the positive and negative optimal values of criterion  $j$ , respectively.

Step 5: Determine  $S_i^+$  and  $S_i^-$  follow the formula:

$$S^+ = \sqrt{\sum_{j=1}^n (k_{ij} - k_j^+)^2} \quad i = 1, 2, \dots, m \quad (20)$$

$$S^- = \sqrt{\sum_{j=1}^n (k_{ij} - k_j^-)^2} \quad i = 1, 2, \dots, m \quad (21)$$

Step 6: Calculate the tight coefficient  $C_i^*$  according to the formula:

$$C_i = \frac{S_i^-}{S_i^+ + S_i^-} \quad i = 1, 2, \dots, m; \quad 0 \leq C_i \leq 1 \quad (22)$$

Step 7: Rank the options according to the  $C_i^*$  highest value as the best.

### 3.4 Confirm optimal results

The smaller the objective is the better was determined as following:

$$S/N = -10 \log \left( \frac{1}{n} \sum_{i=1}^n \frac{1}{y_i} \right) \quad (23)$$

where,  $y_i$  is GRG or  $C_i$  values.

Determine the forecasted value of GRG:

$$\mu_G = G_m + \sum_{i=1}^q (G_0 - G_m) \quad (24)$$

Compute CI value at  $\alpha=0.05$  by employing Eq. (25)

$$CI_{CE} = \pm \sqrt{F_\alpha(1, fe) Ve \left( \frac{1}{n_{eff}} + \frac{1}{R_e} \right)} \quad (25)$$

The  $F_\alpha(1, fe)$  was obtained from Table B-2 in reference [42].

## 4. RESULTS AND DISCUSSION

### 4.1 Design and simulation results

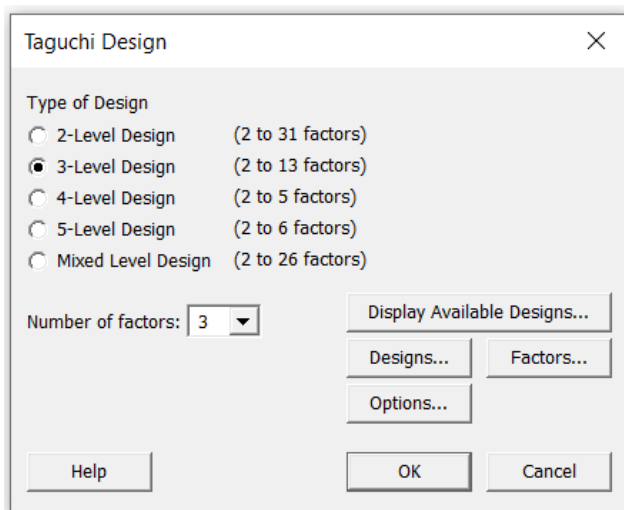
In this study, the force to choose the design variables is the cross-section of box stainless steel for car body 20 mm×30 mm, 20 mm×35 mm, 20 mm×40 mm is the x variable, the thickness of box stainless steel for car body is 1.0 mm, 1.2 mm and 1.4 mm. is the y variable, Z variable is the cross section for the detail to install the 25×25, 25×30, 25×35 vehicle arms as shown in Table 2.

**Table 2.** Design variables and levels

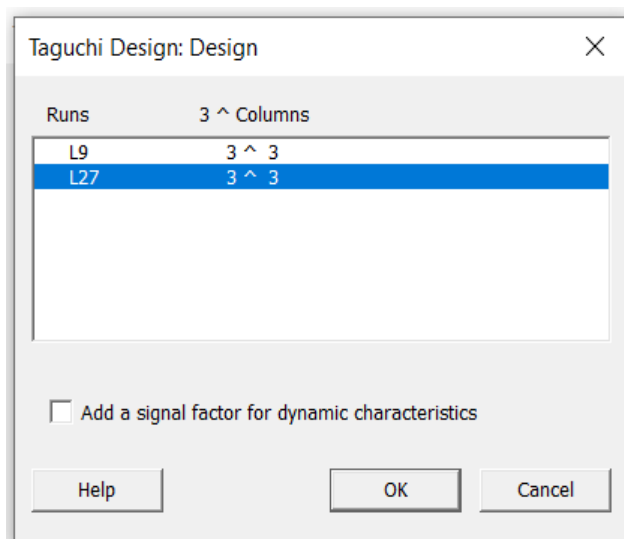
Factor	Unit	Level 1	Level 2	Level 3
x	mm <sup>2</sup>	20×30	20×35	20×40
y	mm	1.0	1.2	1.4
z	mm	25×25	25×30	25×35
t	mm	1.1	1.3	1.5

Then use MiniTab software to design 27 cases for simulation, setup steps are as shown in Figure 3.

Step 2: Go to Designs: select orthogonal array L27 -> OK as shown in Figure 4.



**Figure 3.** Choose the level and number of variables



**Figure 4.** Choose orthogonal array

All shown in Table 3, the simulation results of strain and stress of the vehicle body show that for different cases the strain and stress results are different, proving that design variables influence the significantly to the strain and stress of the vehicle body. Therefore, when designing the vehicle body, the selection of these design variables cannot be ignored. The important thing to consider is that the initial motion of the car body in the x direction is 100t (t is time) mm, the movement in the y direction is 20+50t mm and the vehicle's axle rotates around the z axis at an angle of 40t. degree.

**Table 3.** Orthogonal array and simulation results in transient dynamic

Experiment Order	x	y	z	t	Strain (mm)	Stress (MPa)
1	30	1.0	25	1.2	0.000790	133.430
2	30	1.0	30	1.4	0.000717	130.650
3	30	1.0	35	1.6	0.000681	129.630
4	30	1.2	25	1.4	0.000726	126.490
5	30	1.2	30	1.6	0.000687	128.810
6	30	1.2	35	1.2	0.000650	122.340
7	30	1.4	25	1.6	0.000693	124.870
8	30	1.4	30	1.2	0.000657	117.860
9	30	1.4	35	1.4	0.000718	120.570
10	35	1.0	25	1.2	0.000707	127.480
11	35	1.0	30	1.4	0.000675	125.440
12	35	1.0	35	1.6	0.000661	121.580
13	35	1.2	25	1.4	0.000686	123.580
14	35	1.2	30	1.6	0.000652	119.130
15	35	1.2	35	1.2	0.000615	130.530
16	35	1.4	25	1.6	0.000620	118.660
17	35	1.4	30	1.2	0.000606	114.580
18	35	1.4	35	1.4	0.000562	103.540
19	40	1.0	25	1.2	0.000556	122.490
20	40	1.0	30	1.4	0.000565	105.740
21	40	1.0	35	1.6	0.000531	126.420
22	40	1.2	25	1.4	0.000524	102.550
23	40	1.2	30	1.6	0.000516	125.530
24	40	1.2	35	1.2	0.000490	101.380
25	40	1.4	25	1.6	0.000480	108.470
26	40	1.4	30	1.2	0.000450	106.460
27	40	1.4	35	1.4	0.000436	85.756

### 4.2 Calculate weights for criteria according to MEREC method

In this study, the weights of strain and stress of the vehicle body are determined using the MEREC method. The results of this method are obtained by Eq. (1) to Eq. (6) by substituting the strain value with the stress and Eq. (1) and Eq. (2) as presented in Table 4. The weighted results of strain and stress achieved are 0.4479 and 0.5521, respectively. This result is used for the grey relationship analysis method and the TOPSIS method.

### 4.3 Results of grey relational analysis

Apply Eq. (7) to Eq. (20) into Excel software to perform steps to calculate the optimal value using grey relationship analysis. The results of the objective function, deviation, grey coefficient and grey level obtained and the rank of the grey level are presented in Table 5. As this table shown, the optimal value is case 27 which is the case with the largest grey level. The optimal values of strain and stress are 0.000436 mm and 85.757 MPa, respectively.



**4.4 TOPSIS analysis results**

TOPSIS analysis results are performed by substituting all the results of 27 strain and stress cases into Eq. (15) and Eq. (16), and the results are presented in Table 6. The value  $C_i^*$  is

ranked according to the largest value criterion which is rank 1 and is also the optimal case. This result also confirms that design variables have a significant influence on wheelchair strain and stress.

**Table 4.** Results of MEREC method

Experiment Order	Hij		Si	Sij'		Ej	
	Str	St		Str	St	Str	St
1	1.0000	1.0000	0.0000	0.0000	0.0000	0.0000	0.0000
2	0.9076	0.9792	0.0573	0.0473	0.0105	0.0100	0.0369
3	0.8620	0.9715	0.0850	0.0716	0.0143	0.0134	0.0573
4	0.9190	0.9480	0.0667	0.0414	0.0264	0.0253	0.0150
5	0.8696	0.9654	0.0839	0.0675	0.0175	0.0163	0.0501
6	0.8228	0.9169	0.1318	0.0931	0.0425	0.0388	0.0506
7	0.8772	0.9358	0.0941	0.0634	0.0326	0.0306	0.0308
8	0.8316	0.8833	0.1434	0.0882	0.0602	0.0552	0.0280
9	0.9089	0.9036	0.0939	0.0467	0.0494	0.0472	0.0028
10	0.8949	0.9554	0.0754	0.0540	0.0226	0.0214	0.0315
11	0.8544	0.9401	0.1039	0.0757	0.0304	0.0282	0.0453
12	0.8367	0.9112	0.1272	0.0854	0.0455	0.0418	0.0399
13	0.8684	0.9262	0.1034	0.0682	0.0376	0.0352	0.0306
14	0.8253	0.8928	0.1421	0.0917	0.0551	0.0504	0.0365
15	0.7785	0.9783	0.1277	0.1180	0.0109	0.0097	0.1070
16	0.7848	0.8893	0.1654	0.1144	0.0570	0.0510	0.0574
17	0.7671	0.8587	0.1896	0.1245	0.0734	0.0651	0.0511
18	0.7114	0.7760	0.2601	0.1572	0.1194	0.1029	0.0378
19	0.7038	0.9180	0.1975	0.1618	0.0419	0.0357	0.1199
20	0.7152	0.7925	0.2499	0.1550	0.1100	0.0949	0.0449
21	0.6722	0.9475	0.2034	0.1812	0.0266	0.0223	0.1546
22	0.6633	0.7686	0.2903	0.1867	0.1236	0.1036	0.0631
23	0.6532	0.9408	0.2179	0.1931	0.0301	0.0248	0.1630
24	0.6203	0.7598	0.3193	0.2142	0.1287	0.1051	0.0855
25	0.6076	0.8129	0.3021	0.2224	0.0985	0.0796	0.1239
26	0.5696	0.7979	0.3324	0.2479	0.1070	0.0844	0.1410
27	0.5519	0.6427	0.4175	0.2602	0.1997	0.1573	0.0605

**Table 5.** Result of objective function, deviation, grey coefficient, grey relational grade and rank of grey relational grade

Experiment Order	$D_i^*(1)$	$D_i^*(2)$	$\Delta_{oi}(1)$	$\Delta_{oi}(2)$	$\gamma_i(1)$	$\gamma_i(2)$	$\psi_i$	Rank
1	0.0000	0.0000	1.0000	1.0000	0.3333	0.3333	0.3333	27
2	0.2060	0.0580	0.7940	0.9420	0.3864	0.3467	0.3645	26
3	0.3080	0.0800	0.6920	0.9200	0.4195	0.3521	0.3823	22
4	0.1810	0.1460	0.8190	0.8540	0.3791	0.3693	0.3737	25
5	0.2910	0.0970	0.7090	0.9030	0.4136	0.3564	0.3820	21
6	0.3950	0.2330	0.6050	0.7670	0.4525	0.3946	0.4205	15
7	0.2740	0.1800	0.7260	0.8200	0.4078	0.3788	0.3918	18
8	0.3760	0.3270	0.6240	0.6730	0.4448	0.4263	0.4346	13
9	0.2030	0.2700	0.7970	0.7300	0.3855	0.4065	0.3971	24
10	0.2340	0.1250	0.7660	0.8750	0.3949	0.3636	0.3776	23
11	0.3250	0.1680	0.6750	0.8320	0.4255	0.3754	0.3978	20
12	0.3640	0.2490	0.6360	0.7510	0.4401	0.3997	0.4178	17
13	0.2940	0.2070	0.7060	0.7930	0.4146	0.3867	0.3992	19
14	0.3900	0.3000	0.6100	0.7000	0.4505	0.4167	0.4318	16
15	0.4940	0.0610	0.5060	0.9390	0.4970	0.3475	0.4145	14
16	0.4800	0.3100	0.5200	0.6900	0.4902	0.4202	0.4516	12
17	0.5200	0.3950	0.4800	0.6050	0.5102	0.4525	0.4783	11
18	0.6440	0.6270	0.3560	0.3730	0.5841	0.5727	0.5778	7
19	0.6610	0.2290	0.3390	0.7710	0.5959	0.3934	0.4841	10
20	0.6360	0.5810	0.3640	0.4190	0.5787	0.5441	0.5596	9
21	0.7320	0.1470	0.2680	0.8530	0.6510	0.3695	0.4956	6
22	0.7510	0.6480	0.2490	0.3520	0.6676	0.5869	0.6230	8
23	0.7740	0.1660	0.2260	0.8340	0.6887	0.3748	0.5154	5
24	0.8470	0.6720	0.1530	0.3280	0.7657	0.6039	0.6764	4
25	0.8760	0.5240	0.1240	0.4760	0.8013	0.5123	0.6417	2
26	0.9600	0.5660	0.0400	0.4340	0.9259	0.5353	0.7102	3
27	1.0000	1.0000	0.0000	0.0000	1.0000	1.0000	1.0000	1

**Table 6.** TOPSIS analysis results

TT	Kij		Wij		Si+	Si-	Ci*	Rank
	Di	St	Di	St				
1	0.2438	0.2154	0.1092	0.11894	0.0648	0.0000	0.0000	27
2	0.2213	0.2109	0.0991	0.1165	0.0558	0.0104	0.1571	26
3	0.2102	0.2093	0.0941	0.1156	0.0517	0.0154	0.2299	22
4	0.2241	0.2042	0.1004	0.1128	0.0541	0.0108	0.1664	25
5	0.2120	0.2080	0.0950	0.1148	0.0517	0.0148	0.2227	23
6	0.2006	0.1975	0.0898	0.1091	0.0440	0.0217	0.3305	16
7	0.2139	0.2016	0.0958	0.1113	0.0498	0.0154	0.2366	20
8	0.2028	0.1903	0.0908	0.1051	0.0419	0.0230	0.3550	13
9	0.2216	0.1947	0.0992	0.1075	0.0498	0.0152	0.2335	21
10	0.2182	0.2058	0.0977	0.1136	0.0528	0.0126	0.1932	24
11	0.2083	0.2025	0.0933	0.1118	0.0484	0.0174	0.2646	18
12	0.2040	0.1963	0.0914	0.1084	0.0446	0.0207	0.3174	17
13	0.2117	0.1995	0.0948	0.1102	0.0483	0.0168	0.2587	19
14	0.2012	0.1923	0.0901	0.1062	0.0421	0.0229	0.3525	14
15	0.1898	0.2107	0.0850	0.1164	0.0470	0.0243	0.3413	15
16	0.1913	0.1916	0.0857	0.1058	0.0388	0.0269	0.4096	12
17	0.1870	0.1850	0.0838	0.1021	0.0348	0.0305	0.4668	11
18	0.1734	0.1672	0.0777	0.0923	0.0236	0.0413	0.6367	6
19	0.1716	0.1978	0.0769	0.1092	0.0367	0.0338	0.4793	10
20	0.1744	0.1707	0.0781	0.0943	0.0252	0.0397	0.6117	7
21	0.1639	0.2041	0.0734	0.1127	0.0386	0.0363	0.4852	9
22	0.1617	0.1656	0.0724	0.0914	0.0193	0.0459	0.7042	4
23	0.1592	0.2027	0.0713	0.1119	0.0371	0.0385	0.5092	8
24	0.1512	0.1637	0.0677	0.0904	0.0158	0.0504	0.7612	2
25	0.1481	0.1751	0.0663	0.0967	0.0211	0.0483	0.6955	5
26	0.1389	0.1719	0.0622	0.0949	0.0186	0.0528	0.7399	3
27	0.1346	0.1385	0.0603	0.0764	0.0000	0.0648	1.0000	1

**Table 7.** Mean of signal to noise ratios of GRG

Level	x	y	z	t
1	-8.277	-7.572	-7.093	-6.610
2	-7.227	-6.735	-6.649	-6.137
3	-4.170	-5.367	-5.932	-6.926
Delta	4.107	2.205	1.161	0.789
Rank	1	2	3	4

**Table 8.** Mean of signal to noise ratios of Ci

Level	x	y	z	t
1	-26.804	-24.620	-23.829	-22.247
2	-9.359	-8.851	-8.677	-8.758
3	-3.776	-6.468	-7.433	-8.935
Delta	23.028	18.152	16.396	13.490
Rank	1	2	3	4

**Table 9.** Means of GRG

Level	x	y	z	t
1	0.3866	0.4236	0.4529	0.4811
2	0.4385	0.4707	0.4749	0.5214
3	0.6340	0.5648	0.5313	0.4567
Delta	0.2474	0.1412	0.0784	0.0648
Rank	1	2	3	4

**Table 10.** Means of Ci

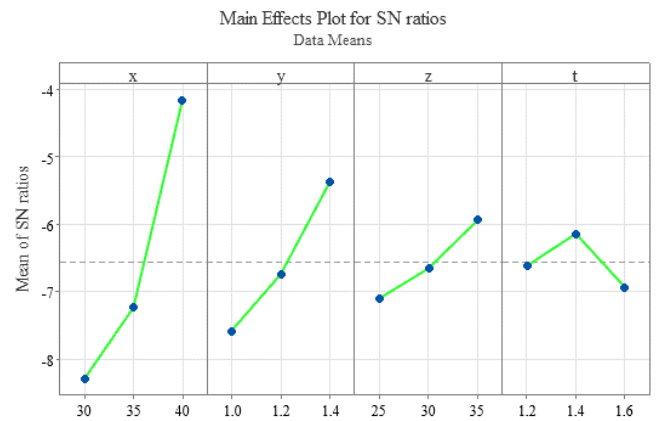
Level	x	y	z	t
1	0.2146	0.3043	0.3493	0.4074
2	0.3601	0.4052	0.4088	0.4481
3	0.6651	0.5304	0.4817	0.3843
Delta	0.4505	0.2261	0.1325	0.0638
Rank	1	2	3	4

**4.5 Taguchi method results**

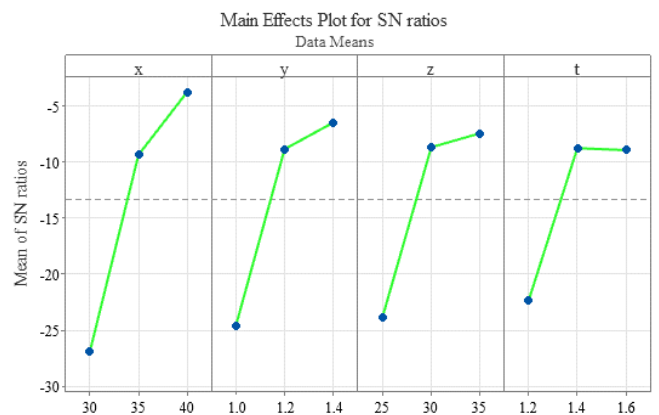
The signal to noise ratios analysis results of GRG and  $C_i$  were presented in Table 7 and Table 8. The 2 tables indicated that the dimension x, y, z and t have significantly changed on the strain and stress of the vehicle frame. where the x dimension was ranked 1, the y dimension was ranked 2, the z dimension was ranked 3, the t dimension was ranked 4. This ranking is according to the largest delta value which was ranked 1 and the next value is ranked 2 until the last value is ranked 4.

Besides, the designed dimension x, y, z and t affected on the GRG and  $C_i$  values are all the same in Tables 7 and 8. The values in two tables were used to draw two the plots as shown in Figure 5 and Figure 6. The GRG graph and  $C_i$  graph confirmed that the case 27<sup>th</sup> is the optimal case. Because the highest peaks of the graph in terms of x, y, z, t variables are 40 mm, 1.4 mm, 35 mm and 1.4 mm respectively. The signal to noise ratios maximum values of GRG and  $C_i$  obtained at the positions x3, y3, z3 and t2. Accordingly, the optimal values of strain and stress are 0.000436 mm and 85.756 MPa respectively.

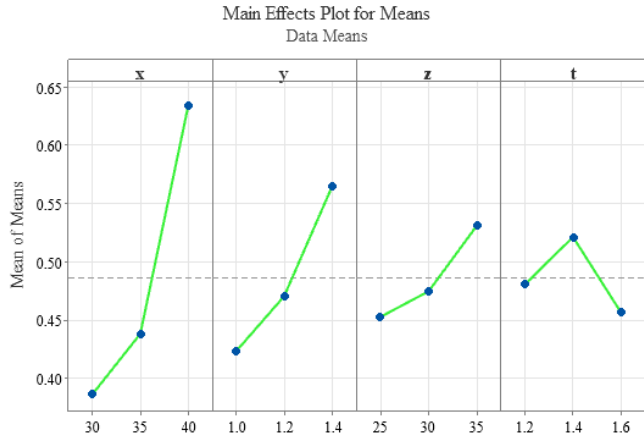
The mean values of GRG and  $C_i$  according to every level of the designed dimension x, y, z and t as illustrate in Table 9 and Table 10. The mean analysis results are similar to the signal to noise analysis results, also indicating the influence of the designed dimensions on GRG and  $C_i$ . This shown that the designed dimensions have significantly changed the strain and stress of the vehicle frame. The optimal case achieved is also case 27<sup>th</sup>. Because the maximum mean values of GRG and  $C_i$  are achieved at positions x3, y3, z3 and t2. The optimal values of GRG and  $C_i$  are both equal to 1. The optimal values of strain and stress are 0.000436 mm and 85.756 MPa, respectively.



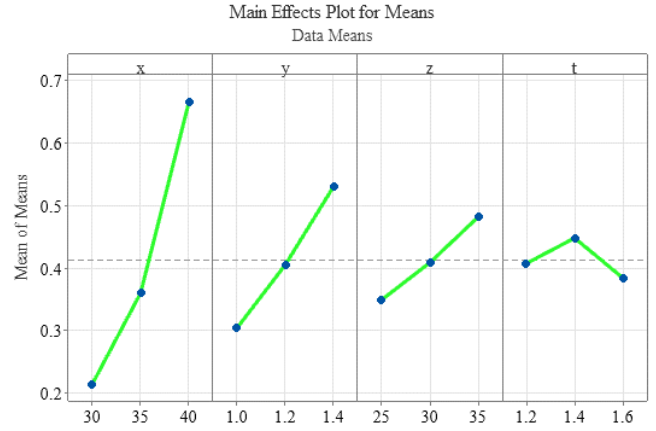
**Figure 5.** The S/N graph of GRG



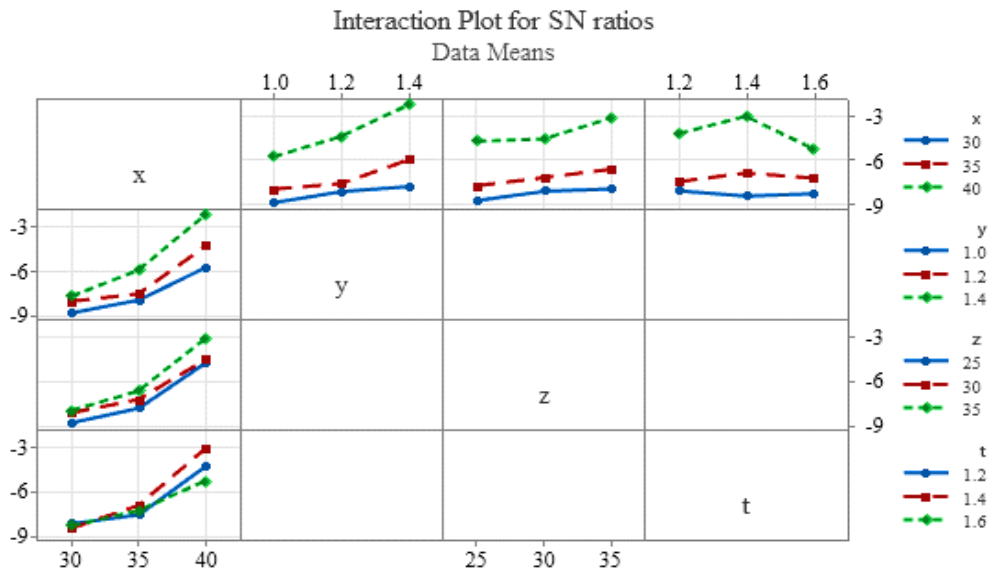
**Figure 6.** The S/N graph of  $C_i$



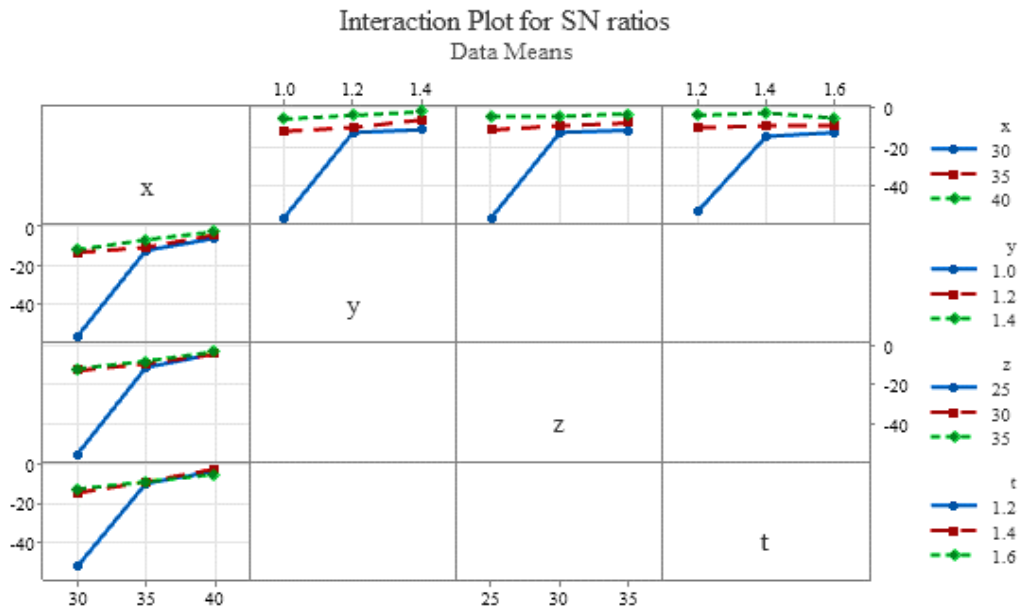
**Figure 7.** The mean graph of GRG



**Figure 8.** The mean graph of  $C_i$



**Figure 9.** The interaction analysis of S/N graph of GRG



**Figure 10.** The interaction analysis of S/N graph of  $C_i$

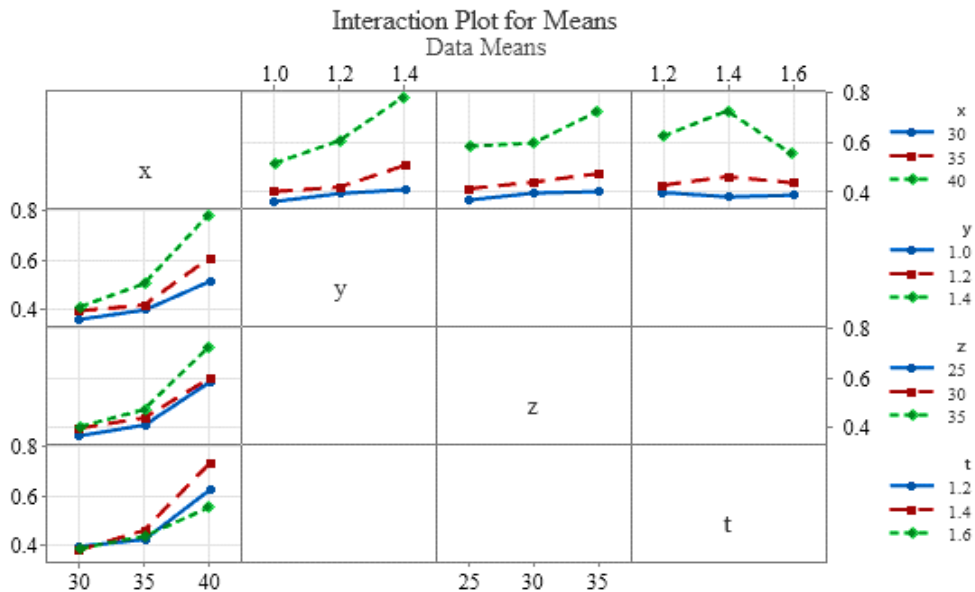


Figure 11. The interaction analysis of mean graph of GRG

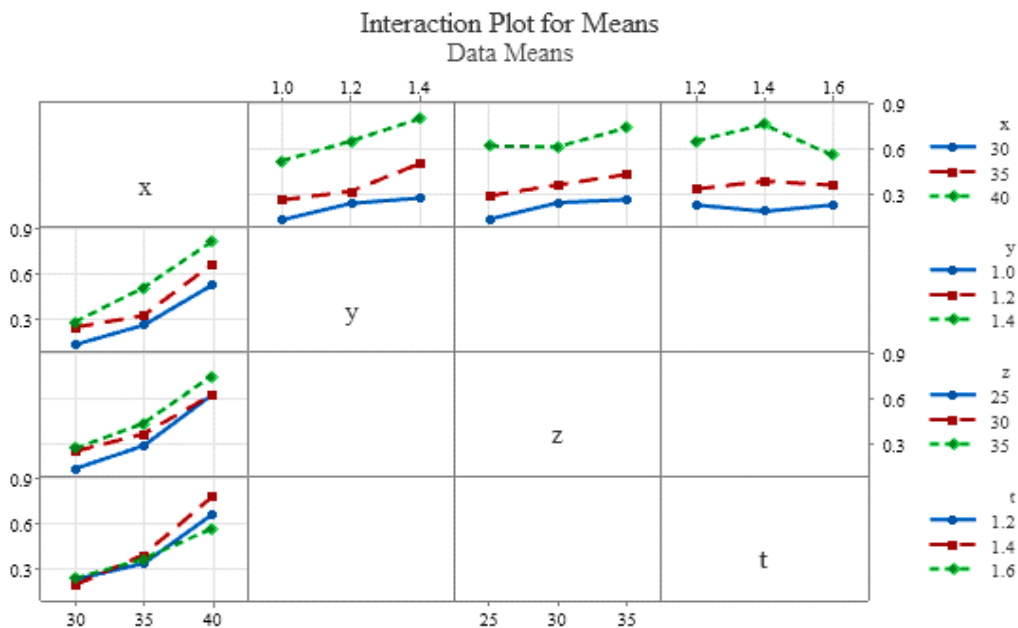


Figure 12. The interaction analysis of mean graph of  $C_i$

The data in Table 9 and Table 10 were utilized to draw the mean plot of GRG and  $C_i$  as pointed out in Figure 7 and Figure 8. In two Figure were also verified that the peaks of the graph at which the optimal levels of the designed dimensions are  $x_3$ ,  $y_3$ ,  $z_3$  and  $t_2$ . And optimal average values of GRG at levels are 0.6340, 0.5648, 0.5313 and 0.5214, respectively. And optimal average values of  $C_i$  at levels are 0.6651, 0.5304, 0.4817, 0.4481, respectively. The optimal values of strain and stress are also 0.000436 mm and 85.756 MPa, respectively.

The interaction analysis of S/N of GRG and  $C_i$  as presented in Figure 9 and Figure 10. From the plots were shown that the design dimensions significantly changed the GRG values, the  $C_i$  values or the strain values and the stress values. Because the interaction graphs are not parallel when the designed dimensions changed. In addition, the graphs also pointed out that the designed dimension (x) significantly changes GRG,  $C_i$  or strain and stress, followed by the designed dimension (y), the designed dimension (z) and finally the designed dimension

(t). The interaction analysis of mean graph as illustrated in Figure 11 and Figure 12. From the plots were shown that the design dimensions significantly change the GRG values, the  $C_i$  values or the strain values and the stress values. Because the interaction graphs are not parallel when the designed dimensions changed. In addition, the graphs also pointed out that the designed dimension (x) significantly changes GRG,  $C_i$  or strain and stress, followed by the designed dimension (y), the designed dimension (z) and finally the designed dimension (t). Because the steeper the slope of the graph, the stronger the influence of the designed dimensions.

The ANOVA results of GRG are recorded in Table 11. Through the percentage contribution of the design dimensions such as x dimension contributes 56%, y dimension contributes 17.05%, z dimension contributes 5.4%, t dimension contributes 3.53%. These values proved that the design dimensions significantly change the strain and stress as stated in the finite element analysis, gray relation analysis results,

TOPSIS results, S/N analysis results, mean analysis results and interaction analysis results. This is also confirmed by the P test and F test. Because the P values all satisfy the condition of being less than 0.05 and the F values all satisfy the condition of being greater than 2. The error of the variance analysis result is 1.66%. The adj Ms value obtained 0.001508. The R-square values are presented in Table 12. All these values are satisfactory. Because all these values are greater than 94%.

The normal probability graph as shown in Figure 13. The horizontal axis shows the expected values or confidence intervals. The vertical axis shows the actual values of GRG. This graph shows that the GRG data are normally distributed. Because the GRG values are all on or near the diagonal. The versus fits plot as shown in Figure 13, the horizontal axis represents the predicted value of GRG, the vertical axis represents the error value between the predicted value and the actual value. From the plot, it can be seen that the error is very small, ranging from -0.02 to 0.04. This problem indicated that

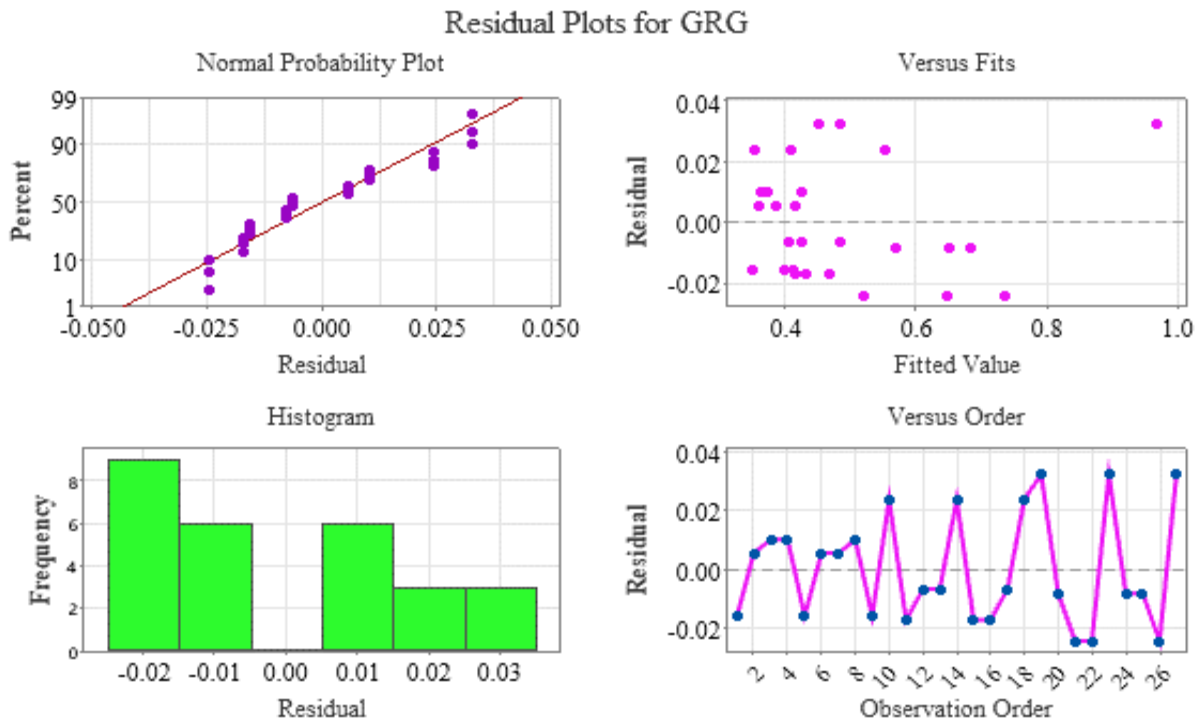
the predicted values of GRG different from the actual values have very low errors. Because the error values are all around the horizontal line at 0 and there is no obvious pattern. The frequency graph pointed out the relationship between the error between the forecast value of GRG and the actual value of GRG and the recurrence frequency. The vertical axis is the recurrence frequency of the error. The horizontal axis is the error value. According to the graph, the error of -0.02 has a higher recurrence frequency than the remaining error values. The problem proved that the predicted model has error is very low. In order test the randomness and sequentially of the GRG data set. The horizontal axis represents the order of the experiments the vertical axis represents the error of the GRG forecast values. According to the graph, the error value of the forecast model of 27 cases with the error is between -0.02 and 0.04. This value is very low. This problem was also demonstrated that the strain and stress prediction model had very low error.

**Table 11.** The result of analysis of variance of GRG

Source	DF	Seq SS	Contribution	Adj SS	Adj MS	F-Value	P-Value
x	2	0.306311	56.15%	0.306311	0.153156	101.55	0.000
y	2	0.092993	17.05%	0.092993	0.046496	30.83	0.001
z	2	0.029454	5.40%	0.029454	0.014727	9.76	0.013
t	2	0.019249	3.53%	0.019249	0.009624	6.38	0.033
x*y	4	0.043383	7.95%	0.043383	0.010846	7.19	0.018
x*z	4	0.014655	2.69%	0.014655	0.003664	2.43	0.159
x*t	4	0.030443	5.58%	0.030443	0.007611	5.05	0.040
Error	6	0.009049	1.66%	0.009049	0.001508		
Total	26	0.545537	100.00%				

**Table 12.** Model summary of GRG

S	R-sq	R-sq(adj)	PRESS	R-sq(pred)	AICc	BIC
0.0388355	98.34%	96.81%	0.183246	94.41%	157.60	-66.89



**Figure 13.** Statistical analysis graph of GRG



The ANOVA results of  $C_i$  are recorded in Table 13. Through the percentage contribution of the design dimensions such as x dimension contributes 67%, y dimension contributes 16.49%, z dimension contributes 5.66%, t dimension contributes 1.34%. These values proved that the design dimensions significantly changed on the strain and stress as stated in the finite element analysis, grey relation analysis results, TOPSIS results, S/N analysis results, mean analysis results and interaction analysis results. These problems were also confirmed by the P test and F test. Because the P values all satisfy the condition of being less than 0.05 and the F values all satisfy the condition of being greater than 2. The error of the variance analysis result is 1.88%. The adj Ms value obtained 0.004384. The R-square values are presented in Table 14. All these values are satisfactory. Because all these values are greater than 94%.

The normal probability graph as shown in Figure 14. The horizontal axis shows the expected values or confidence intervals. The vertical axis shows the actual values of  $C_i$ . This graph shows that the  $C_i$  data are normally distributed. Because the  $C_i$  values are all on or near the diagonal. The versus fits plot as shown in Figure 14, the horizontal axis represents the

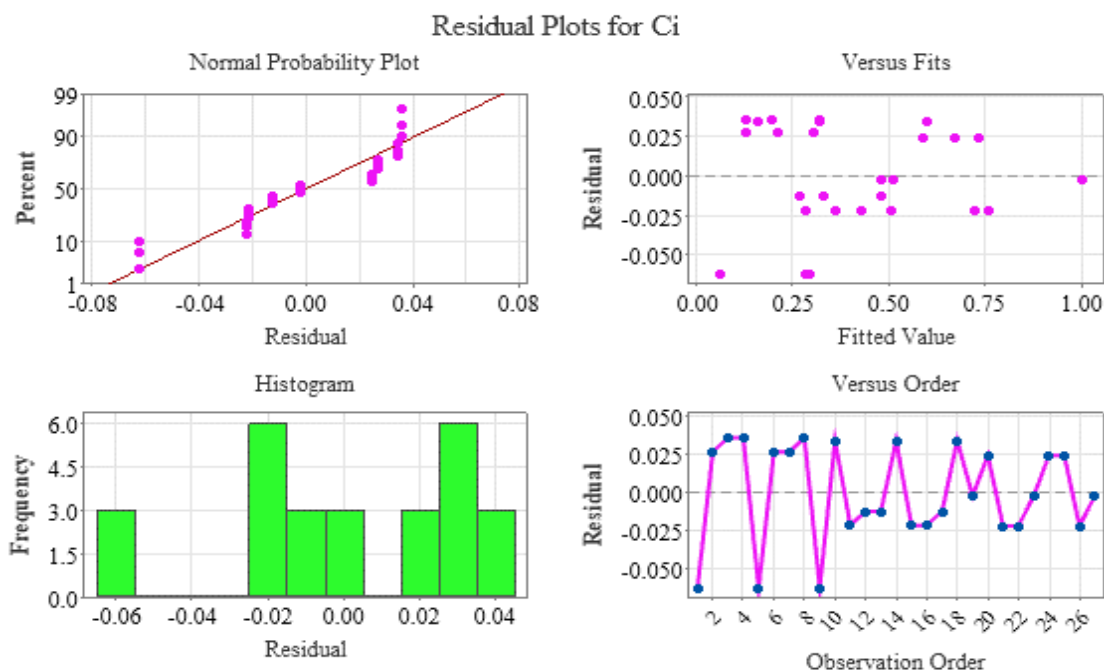
predicted value of  $C_i$ , the vertical axis represents the error value between the predicted value and the actual value. From the plot, it can be seen that the error is very small, ranging from -0.05 to 0.05. This problem indicated that the predicted values of GRG different from the actual values have very low errors. Because the error values are all around the horizontal line at 0 and there is no obvious pattern. The frequency graph pointed out the relationship between the error between the forecast value of  $C_i$  and the actual value of  $C_i$  and the recurrence frequency. The vertical axis is the recurrence frequency of the error. The horizontal axis is the error value. According to the graph, the error of -0.05 and 0.05 has a higher recurrence frequency than the remaining error values. The problem proved that the predicted model has error is very low. In order test the randomness and sequentially of the  $C_i$  data set. The horizontal axis represents the order of the experiments the vertical axis represents the error of the  $C_i$  forecast values. According to the graph, the error value of the forecast model of 27 cases with the error is between -0.05 and 0.05. This value is very low. This problem was also demonstrated that the strain and stress prediction model had very low error.

**Table 13.** Analysis of variance of  $C_i$

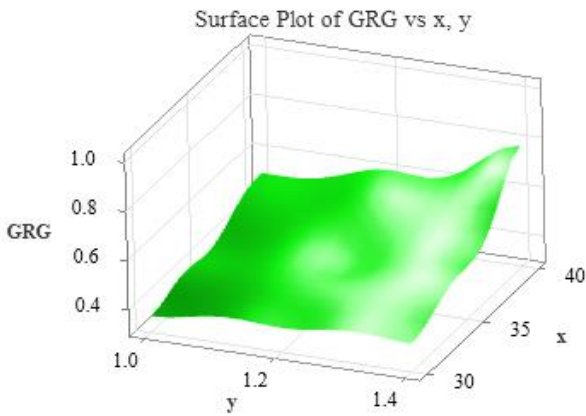
Source	DF	Seq SS	Contribution	Adj SS	Adj MS	F-Value	P-Value
x	2	0.95152	67.93%	0.95152	0.475761	110.52	0.000
y	2	0.23101	16.49%	0.23101	0.115504	28.35	0.001
z	2	0.07923	5.66%	0.07923	0.039613	9.04	0.015
t	2	0.01879	1.34%	0.01879	0.009393	4.14	0.019
x*y	4	0.02602	1.86%	0.02602	0.006505	3.48	0.031
x*z	4	0.01331	0.95%	0.01331	0.003327	2.76	0.049
x*t	4	0.05463	3.90%	0.05463	0.013658	5.12	0.014
Error	6	0.02630	1.88%	0.02630	0.004384		
Total	26	1.40080	100.00%				

**Table 14.** Model summary of  $C_i$

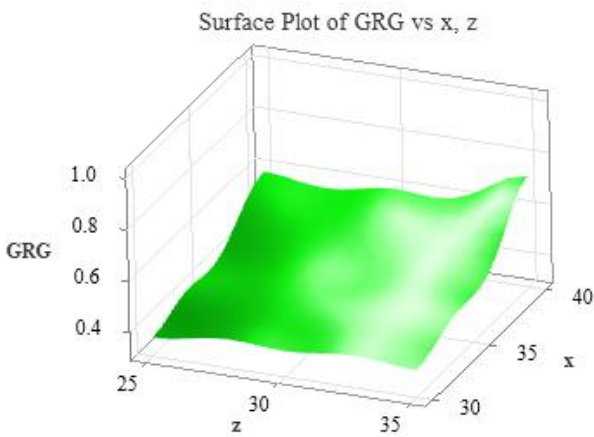
S	R-sq	R-sq(adj)	PRESS	R-sq(pred)	AICc	BIC
0.0662126	98.12%	96.86%	0.532669	94.97%	186.41	-68.08



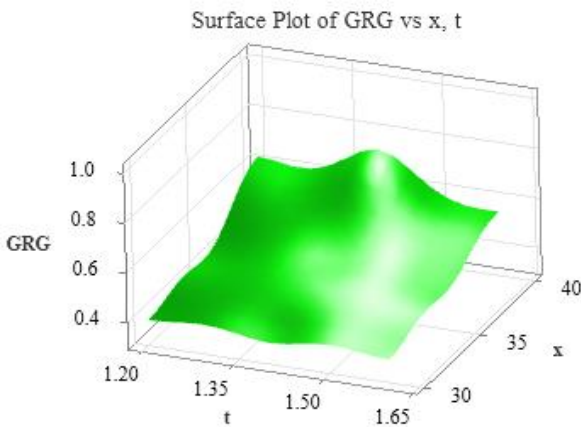
**Figure 14.** Statistical analysis graph of  $C_i$



**Figure 15.** Graph the relationship between dimensions' x and t with GRG



**Figure 16.** Graph the relationship between dimensions x and z with GRG



**Figure 17.** Graph the relationship between dimensions' x and t with GRG

#### 4.6 Result of 3D surface plot

The relationship between GRG and the x and y dimensions as shown in Figure 15 indicated that when the x dimension increased from 30 mm to 40 mm and the y dimensions from 1.0 mm to 4.4 mm the GRG values increased. The problem proved that the strain and stress decreased. Because the optimal case is minimum strain and stress or maximum GRG. The relationship between GRG and the x and z dimensions as shown in Figure 16 indicated that when the x dimension

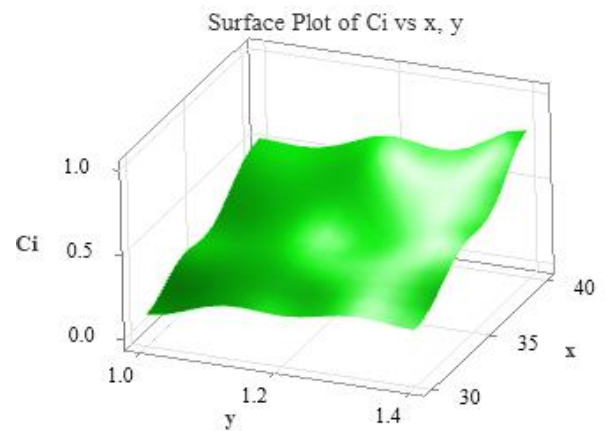
increased from 30 mm to 40 mm and the z dimensions from 25 mm to 35 mm the GRG values increased. The problem proved that the strain and stress decreased. Because the optimal case is minimum strain and stress or maximum GRG.

The relationship between GRG and the x and t dimensions as shown in Figure 17 indicated that when the x dimension increased from 30 mm to 40 mm and the t dimensions from 1.2 mm to 1.6 mm the GRG values increased. The problem proved that the strain and stress decreased. Because the optimal case is minimum strain and stress or maximum GRG.

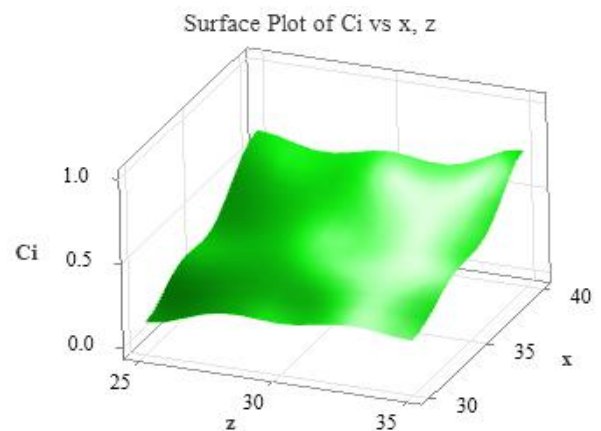
The relationship between  $C_i$  and the x and y dimensions as shown in Figure 18 indicated that when the x dimension increased from 30 mm to 40 mm and the y dimensions from 1.0 mm to 1.4 mm the  $C_i$  values increased. The problem proved that the strain and stress decreased. Because the optimal case is minimum strain and stress or maximum  $C_i$ .

The relationship between  $C_i$  and the x and z dimensions as shown in Figure 19 indicated that when the x dimension increased from 30 mm to 40 mm and the z dimensions from 25 mm to 35 mm the  $C_i$  values increased. The problem proved that the strain and stress decreased. Because the optimal case is minimum strain and stress or maximum  $C_i$ .

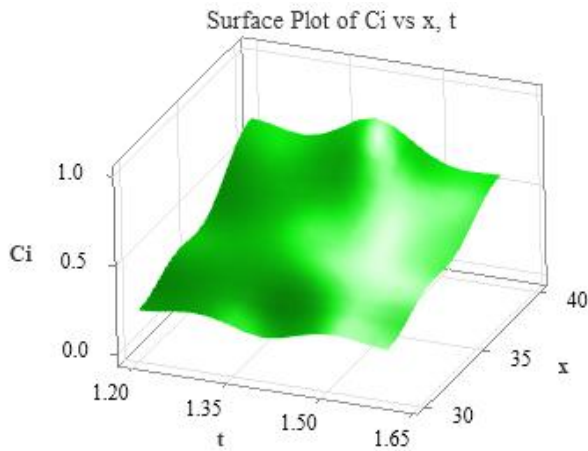
The relationship between  $C_i$  and the x and t dimensions as shown in Figure 20 indicated that when the x dimension increased from 30 mm to 40 mm and the t dimensions from 1.2 mm to 1.6 mm the  $C_i$  values increased. The problem proved that the strain and stress decreased. Because the optimal case is minimum strain and stress or maximum  $C_i$ .



**Figure 18.** Graph the relationship between dimensions x and y with  $C_i^*$



**Figure 19.** Graph the relationship between dimensions x and z with  $C_i^*$



**Figure 20.** Graph the relationship between dimensions x and t with  $C_i^*$

From the results of 3D surface analysis by GRG and  $C_i$  demonstrated that the designed dimensions significantly changed on the GRG values and  $C_i$  values of the strain values and the stress values. These results were consistent with the results of the gray relational analysis, TOPSIS method, Taguchi method, interaction analysis and ANOVA analysis.

#### 4.6 Verify results

For GRG:

$$CI_{CE} = \pm \sqrt{5.9874 \times 0.001508 \times \left( \frac{1}{27} + 1 \right)} = \pm 0.128$$

$$0.8395 < \mu_{confirmation} < 1.0955$$

where,  $\alpha = 0.05$ ,  $fe = 6$ ,  $F_{0.05}(1,6) = 5.9874$  [42],  $Ve = 0.001508$ ,  $R = 21$ ,  $Re = 1$ ,  $n = 27$ .

For  $C_i$ :

$$CI_{CE} = \pm \sqrt{5.9874 \times 0.004384 \times \left( \frac{1}{27} + 1 \right)} = \pm 0.218$$

$$0.784 < \mu_{confirmation} < 1.220$$

where,  $\alpha = 0.05$ ,  $fe = 6$ ,  $F_{0.05}(1,6) = 5.9874$  [42],  $Ve = 0.004384$ ,  $R = 21$ ,  $Re = 1$ ,  $n = 27$ .

From the simulation results through grey relational analysis, the GRG values were determined. These GRG values were compared with the predicted values by using MiniTab software as listed in Table 15. This table indicated that the GRG values obtained from the simulation data and the grey relation analysis method were approximately the same as the value predicted by MiniTab software with very low error. The optimal value of GRG obtained 1 while the predicted value of GRG archived 0.9675 with 3.25% error.

From the simulation results through the make decision TOPSIS method, the  $C_i$  values were determined. These  $C_i$  values were compared with the predicted values by using MiniTab software as listed in Table 16. This table indicated that the  $C_i$  values obtained from the simulation data and the make decision TOPSIS method were approximately the same as the value predicted by MiniTab software with very low error. The optimal value of GRG obtained 1 while the predicted value of GRG archived 1.002 with 0.2% error.

**Table 15.** Comparison between predicted and simulation values of GRG

GRG	Predicted GRG	Error	S/N of GRG	Predicted S/N of GRG	Error
0.3333	0.3491	0.0158	-9.5432	-9.1791	0.3641
0.3645	0.3588	-0.0057	-8.7664	-8.9004	-0.1340
0.3823	0.3720	-0.0103	-8.3521	-8.5824	-0.2303
0.3737	0.3634	-0.0103	-8.5497	-8.7800	-0.2303
0.3820	0.3978	0.0158	-8.3582	-7.9941	0.3641
0.4205	0.4149	-0.0056	-7.5240	-7.6579	-0.1339
0.3918	0.3861	-0.0057	-8.1389	-8.2728	-0.1339
0.4346	0.4243	-0.0103	-7.2384	-7.4687	-0.2303
0.3971	0.4129	0.0158	-8.0221	-7.6579	0.3642
0.3776	0.3536	-0.0240	-8.4589	-8.8467	-0.3878
0.3978	0.4150	0.0172	-8.0058	-7.7119	0.2939
0.4178	0.4245	0.0067	-7.5807	-7.4867	0.0940
0.3992	0.4059	0.0067	-7.9762	-7.8823	0.0939
0.4318	0.4079	-0.0239	-7.2936	-7.6814	-0.3878
0.4145	0.4316	0.0171	-7.6503	-7.3564	0.2939
0.4516	0.4687	0.0171	-6.9058	-6.6119	0.2939
0.4783	0.4850	0.0066	-6.4052	-6.3112	0.0940
0.5778	0.5538	-0.0240	-4.7643	-5.1521	-0.3878
0.4841	0.4516	-0.0325	-6.3013	-6.4517	-0.1504
0.5596	0.5677	0.0081	-5.0424	-5.1152	-0.0728
0.4956	0.5199	0.0243	-6.0977	-5.8745	0.2232
0.6230	0.6474	0.0244	-4.1096	-3.8864	0.2232
0.5154	0.4829	-0.0325	-5.7573	-5.9076	-0.1503
0.6764	0.6844	0.0080	-3.3963	-3.4690	-0.0727
0.6417	0.6498	0.0080	-3.8528	-3.9255	-0.0727
0.7102	0.7346	0.0243	-2.9718	-2.7487	0.2231
1.0000	0.9675	-0.0325	0.0000	-0.1504	-0.1504

**Table 16.** Comparison between predicted and simulation values of  $C_i$ 

$C_i$	Predicted $C_i$	Error	S/N of $C_i$	Predicted S/N of $C_i$	Error
0.0000	-	-	-	-	-
0.1571	0.1302	-0.0268	-16.0791	-27.9225	-11.8434
0.2299	0.194	-0.0358	-12.7698	-24.9039	-12.1341
0.1664	0.1305	-0.0358	-15.5779	-27.7121	-12.1342
0.2227	0.2852	0.0625	-13.0462	10.9313	23.9775
0.3305	0.3037	-0.0267	-9.6176	-21.461	-11.8434
0.2366	0.2098	-0.0268	-12.5195	-24.363	-11.8435
0.3550	0.3191	-0.0358	-8.9962	-21.1304	-12.1342
0.2335	0.2960	0.0625	-12.6330	11.3445	23.9775
0.1932	0.1591	-0.0341	-14.2805	-14.5526	-0.2721
0.2646	0.2862	0.0216	-11.5468	-11.3598	0.1870
0.3174	0.3298	0.0124	-9.9684	-9.8833	0.0851
0.2587	0.2711	0.0124	-11.7455	-11.6604	0.0851
0.3525	0.3184	-0.0341	-9.0578	-9.3297	-0.2719
0.3413	0.3628	0.0215	-9.3381	-9.151	0.1871
0.4096	0.4311	0.0215	-7.7523	-7.5653	0.1870
0.4668	0.4792	0.0124	-6.6173	-6.5322	0.0851
0.6367	0.6026	-0.0341	-3.9216	-4.1937	-0.2721
0.4793	0.4816	0.0023	-6.3884	-6.081	0.3074
0.6117	0.5873	-0.0244	-4.2692	-4.781	-0.5118
0.4852	0.5072	0.0219	-6.2808	-6.0763	0.2045
0.7042	0.7262	0.0219	-3.0455	-2.841	0.2045
0.5092	0.5114	0.0023	-5.863	-5.5558	0.3072
0.7612	0.7368	-0.0244	-2.3704	-2.8823	-0.5119
0.6955	0.6711	-0.0244	-3.1543	-3.6661	-0.5118
0.7399	0.7619	0.0219	-2.6164	-2.4119	0.2045
1.0000	1.0020	0.0020	0.0000	0.3073	0.3073

**Table 17.** Comparison between the predicted and simulation values

Strain	Predicted Strain	Error	Stress	Pre. stress	Error
0.000790	0.000760	-0.000030	133.43	131.899	-1.531
0.000717	0.000732	0.000015	130.65	130.769	0.119
0.000681	0.000695	0.000014	129.63	131.042	1.412
0.000726	0.000740	0.000014	126.49	127.902	1.412
0.000687	0.000657	-0.000030	128.81	127.279	-1.531
0.000650	0.000665	0.000015	122.34	122.459	0.119
0.000693	0.000708	0.000015	124.87	124.989	0.119
0.000657	0.000671	0.000014	117.86	119.272	1.412
0.000718	0.000689	-0.000029	120.57	119.039	-1.531
0.000707	0.000709	0.000002	127.48	131.265	3.785
0.000675	0.000681	0.000006	125.44	121.065	-4.375
0.000661	0.000653	-0.000008	121.58	122.169	0.589
0.000686	0.000678	-0.000008	123.58	124.169	0.589
0.000652	0.000654	0.000002	119.13	122.916	3.786
0.000615	0.000621	0.000006	130.53	126.156	-4.374
0.000620	0.000626	0.000006	118.66	114.286	-4.374
0.000606	0.000598	-0.000008	114.58	115.169	0.589
0.000562	0.000564	0.000002	103.54	107.326	3.786
0.000556	0.000559	0.000003	122.49	120.653	-1.837
0.000565	0.000559	-0.000006	105.74	109.965	4.225
0.000531	0.000534	0.000003	126.42	124.032	-2.388
0.000524	0.000528	0.000004	102.55	100.162	-2.388
0.000516	0.000519	0.000003	125.53	123.693	-1.837
0.000490	0.000484	-0.000006	101.38	105.605	4.225
0.000480	0.000474	-0.000006	108.47	112.695	4.225
0.000450	0.000454	0.000004	106.46	104.072	-2.388
0.000436	0.000439	0.000003	85.756	83.919	-1.837

The error between the predicted and the simulation values of the strain and stress value were very low not exceeding 0.000030 mm and 4.375 MPa, respectively as presented in Table 17. The predicted and optimal values of strain and stress were 0.000436 mm and 85.756 MPa, respectively. The error percentage between the predicted and optimal values of strain and stress were very low not exceeding 0.68% and 2.14%, respectively. The strain and stress results are very low, proving

that the model is durable enough to work and can proceed to manufacture a stair climbing wheelchair model for experimentation.

#### 4.7 Optimal results

The optimal case strain results of the chassis are achieved as shown in Figure 21. The graph in this figure is close to a

periodic function. The optimal strain value of the chassis is 0.000436 mm. This result is very small, ensuring enough durability for the vehicle to go up the stairs under the condition that the vehicle moves in the x direction is 100t mm, moves in the y direction is 20+50t mm and the vehicle axis rotates around the z axis at an angle of 40t degrees.

The optimal case stress results of the vehicle frame are achieved as shown in Figure 22. The graph in this figure is close to a periodic function. The optimal stress value of the vehicle frame is 85,757 MPa. This result is very small, ensuring enough durability for the vehicle to go up the stairs under the condition that the vehicle moves in the x direction is 100t mm, moves in the y direction is 20+50t mm and the vehicle axis rotates around the z axis at an angle of 40t degrees.

The optimal case strain results of the wheel mounting detail are achieved as shown in Figure 23. The optimal strain value of the chassis is 0.000045 mm. This result is very small, ensuring enough durability for the vehicle to go up the stairs under the condition that the vehicle moves in the x direction at 100t mm, moves in the y direction at 20+50t mm and the vehicle axis rotates around the z axis at an angle of 40t degrees.

The optimal case stress result of the wheel mounting detail is achieved as shown in Figure 24. The optimal stress value of the wheel mounting part is 7 MPa. This strain and stress are very small when the car moves up the stairs. Ensure stable operation of the vehicle with the condition that the vehicle moves in the x direction at 100t mm, moves in the y direction at 20+50t mm and the vehicle axle rotates around the z axis at an angle of 40t degrees.

At 9<sup>th</sup> seconds the strain of the chassis is 0.000155 mm. The stress of the chassis is 30.47 MPa as shown in Figure 25 and Figure 26. At time 9<sup>th</sup> seconds, the strain and stress of the wheel mounting part are 0.00000632 mm and 0.898 MPa, as shown in Figure 27 and Figure 28, respectively. This strain and stress are very small, ensuring that the vehicle works well when the vehicle moves up the stairs with the condition that the vehicle moves in the x direction at 100t mm, moves in the y direction at 20+50t mm and the vehicle axle rotates around the z axis 1 40-degree angle.

Dynamic simulation analysis of stair-climbing wheelchairs in ANSYS software is very difficult to perform. Most previous studies have only analyzed the stability in the static state. In this study, we successfully simulated the stability analysis for the wheelchair when climbing stairs through the analysis of stress and relative deformation of the frame and blocking devices. The optimal stair-climbing wheelchair frame structure is achieved based on gray relation analysis, a multi-criteria decision-making method. In addition, the results are also confirmed by the results of signal to noise analysis, means

analysis, interaction analysis, variance analysis, and 3D surface graph analysis.

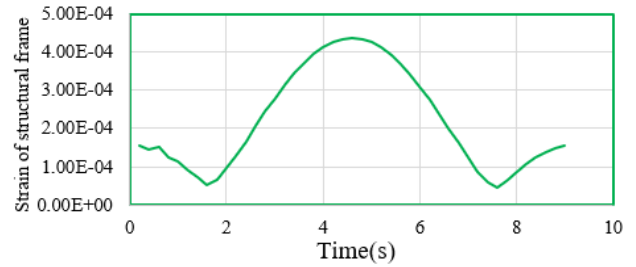


Figure 21. Optimal strain results of the chassis

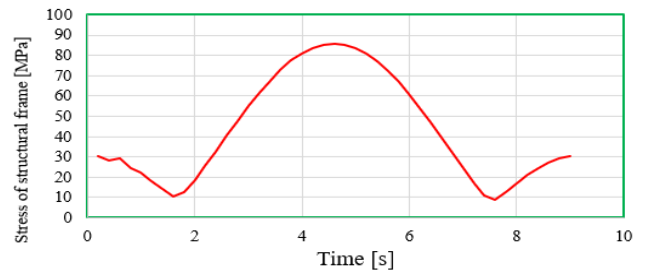


Figure 22. Optimal stress results of the vehicle frame

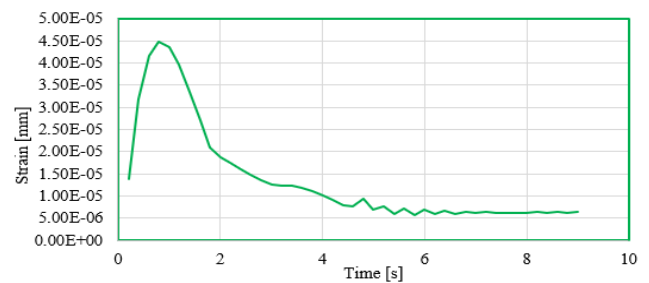


Figure 23. Optimal strain results of wheel mounting details

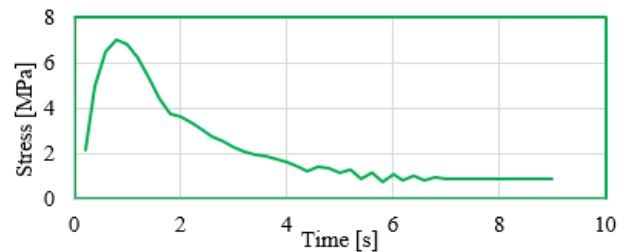


Figure 24. Optimal stress results of wheel mounting details

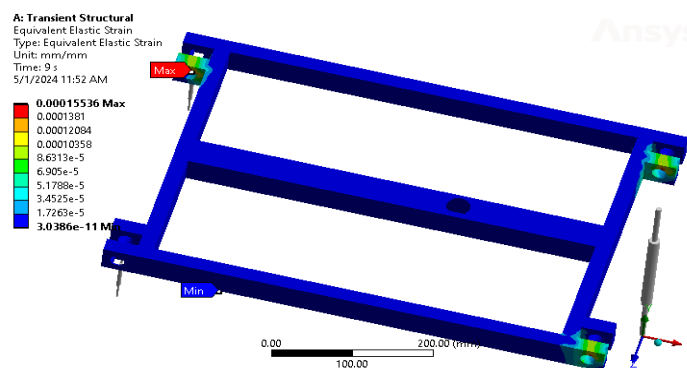


Figure 25. Optimal strain results of the chassis at 9<sup>th</sup> seconds



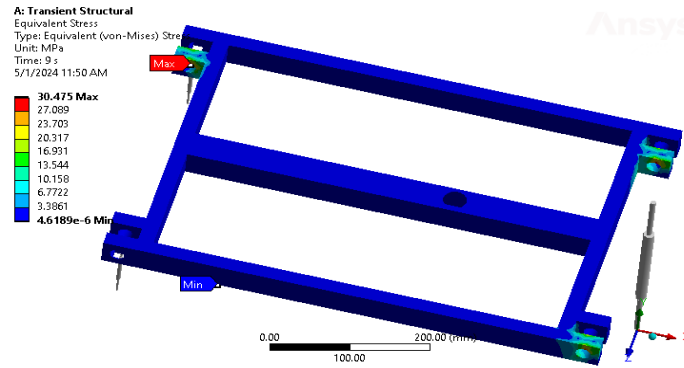


Figure 26. Result of optimal stress of the chassis at 9<sup>th</sup> seconds

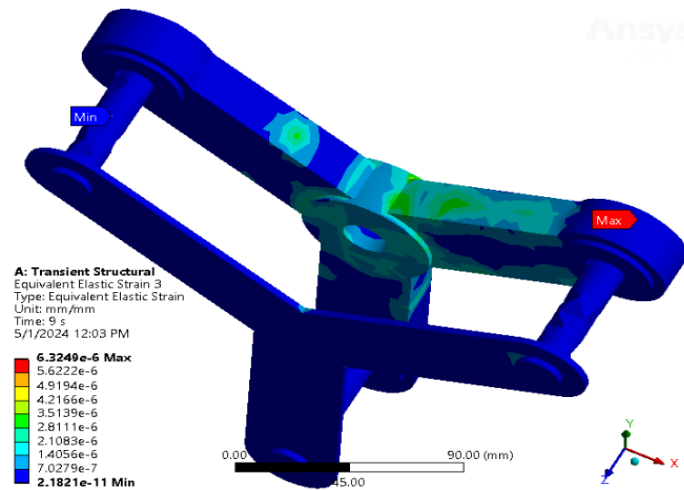


Figure 27. Optimal strain results of wheel mounting parts at 9<sup>th</sup> seconds

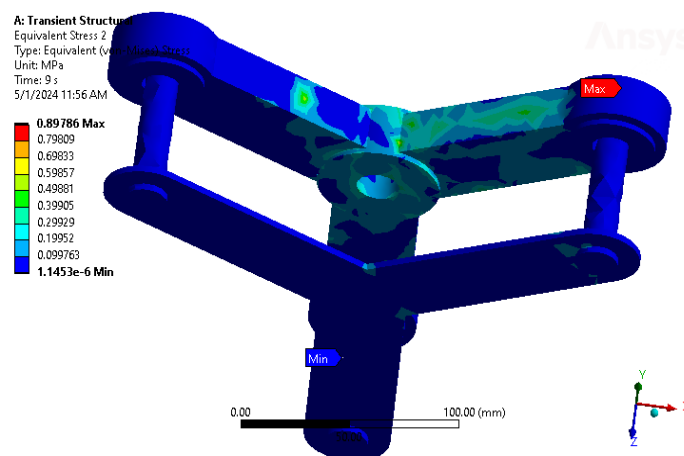


Figure 28. Result of optimal stress of wheel mounting parts at 9<sup>th</sup> seconds

## 5. CONCLUSION

In this study, an optimal wheelchair model was designed with a frame made of SS304 stainless steel with dimensions of 20×40 mm<sup>2</sup> and a thickness of 1.4. This optimal result is achieved by weighted grey relational analysis using the MEREC method based on the results of analyzing the strain and stress of the vehicle while moving up the stairs in the x direction of 100t. The y direction is 20 +50t, and the vehicle axis rotates in the z direction 40t degrees. This result was also

confirmed by the TOPSIS method. The results of finite element analysis while the vehicle is in motion show that design variables significantly affect the stress and strain of the vehicle frame and wheel mounting details. This result contributes to reducing manufacturing costs by determining the optimal case in choosing the vehicle body size to ensure durability of the vehicle body. Reliable optimization method can be applied to general design optimization and structural optimization. Transient analysis results of ANSYS software can be applied to manufacturing. This study provides an

optimal solution for structural design using the data of dynamics analysis by finite element method in ANSYS. The optimization methods confirm the influence of design dimensions on the relative stress and strain of the vehicle frame and blocking devices. Therefore, the error of the model compared to reality has not been determined. To confirm ANSYS analysis results and optimization results need to build a mathematical model for wheelchairs going up stairs and make real models and Automatic control for wheelchair climbing stairs using PLC control algorithm.

## ACKNOWLEDGMENT

This work was financially supported by Ho Chi Minh City University of Industry and Trade under Contract No.: 196/HĐ-DCT dated on 31 Aug., 2023.

## REFERENCES

- [1] Arunkumar, A., Ramabalan, S., Elayaraja, D. (2023). Optimum design of stair-climbing robots using Taguchi method. *Intelligent Automation & Soft Computing*, 35(1): 1229-1244. <https://doi.org/10.32604/iasc.2023.027388>
- [2] Azmin, M.Z., Rahman, W.M.W.W.A. (2023). Improvement of stair climbing trolley. *Progress in Engineering Application and Technology*, 4(1): 714-722.
- [3] Chen, Y., Kuwahara, T., Nishimura, Y., Suzuki, K. (2023). WeMo: A prototype of a wearable mobility device adapting to user's natural posture changes. *Sensors*, 23(18): 7683. <https://doi.org/10.3390/s23187683>
- [4] Eom, S.H., Kang, J.M., Kim, G.Y., Lee, E.H. (2023). A study on gathering staircase information for active staircase entry of wheelchair stair climbing assistive devices. In *Proceedings of the 20th International Conference on Informatics in Control, Automation and Robotics (ICINCO 2023)*, Rome, Italy, pp. 747-753. <https://doi.org/10.5220/0012255700003543>
- [5] Jadhav, D., Kurane, N., Mali, O., Pawar, R., Jadhav, A., Korwar, G. (2023). Design and development of rover with pick and place Mechanism. *Journal of Physics: Conference Series*, 2601(1): 012007. <https://doi.org/10.1088/1742-6596/2601/1/012007>
- [6] Lee, G., Togami, N., Hayakawa, Y., Tamura, H. (2023). Two functional wheel mechanism capable of step ascending for personal mobility aids. *Electronics*, 12(6): 1399. <https://doi.org/10.3390/electronics12061399>
- [7] Olodu, D.D., Abraham, M., Jesuorobo, J., Akiakeme, O.O. (2023). The design and construction of a locally sourced electric powered stair climbing trolley. *Black Sea Journal of Engineering and Science*, 6(1): 25-31. <https://doi.org/10.34248/bsengineering.1187210>
- [8] Ordoñez-Avila, J.L., Moreno, H.A., Perdomo, M.E., Calderón, I.G.C. (2023). Designing legged wheels for stair climbing. *Symmetry*, 15(11): 2071. <https://doi.org/10.3390/sym15112071>
- [9] Pappalètera, A., Bottiglione, F., Mantriota, G., Reina, G. (2023). Watch the next step: A comprehensive survey of stair-climbing vehicles. *Robotics*, 12(3): 74. <https://doi.org/10.3390/robotics12030074>
- [10] Ramadan, M., Hilles, S.M., Alkhedher, M. (2023). Design and study of an ai-powered autonomous stair climbing robot. *El-Cezeri*, 10(3): 571-585. <https://doi.org/10.31202/ecjse.1272769>
- [11] Seo, T., Ryu, S., Won, J.H., Kim, Y., Kim, H.S. (2023). Stair-climbing robots: A review on mechanism, sensing, and performance evaluation. *IEEE Access*, 11: 60539-60561. <https://doi.org/10.1109/access.2023.3286871>
- [12] Zhang, G., Ma, S., Liu, J., Zeng, X., Kong, L., Li, Y. (2023). Q-Whex: A simple and highly mobile quasi-wheeled hexapod robot. *Journal of Field Robotics*, 40(6): 1444-1459. <https://doi.org/10.1002/rob.22186>
- [13] Zhang, Y., Li, Y., Zhang, H., Wang, Y., Wang, Z., Ye, Y., Zhang, S. (2023). Earthshaker: A mobile rescue robot for emergencies and disasters through teleoperation and autonomous navigation. *JUSTC*, 53(1): 1-12. <https://doi.org/10.52396/justc-2022-0066>
- [14] Zhu, Y., Li, H., Lyu, S., Shan, X., Jan, Y.K., Ma, F. (2023). Stair-climbing wheelchair proven to maintain user's body stability based on AnyBody musculoskeletal model and finite element analysis. *PLoS One*, 18(1): e0279478. <https://doi.org/10.1371/journal.pone.0279478>
- [15] Chen, G., Wang, K.C., Wu, L., Zhan, S.Y. (2024). A novel design of a small adaptive bionic obstacle-crossing vehicle. *Sensors and Materials*, 36(6): 2351-2370. <https://doi.org/10.18494/sam4879>
- [16] Chen, W., Zhang, Z. (2024). Kinematic performance analysis of a robot climbing steps without movable tracks on a swing arm. *Journal of Physics: Conference Series*, 2741(1): 012028. <https://doi.org/10.1088/1742-6596/2741/1/012028>
- [17] Majithia, A., Shah, D., Dave, J., Kumar, A., Rathee, S., Dogra, N., Hiremath, S. (2024). Design, motions, capabilities, and applications of quadruped robots: A comprehensive review. *Frontiers in Mechanical Engineering*, 10: 1448681. <https://doi.org/10.3389/fmech.2024.1448681>
- [18] Zhang, K., Sun, X., Li, R., Yu, Z., Yu, B. (2024). A linkage-type self-adaptive deformable tracked mechanism based on the six-bar mechanism. *Mechanical Sciences*, 15(2): 541-553. <https://doi.org/10.5194/ms-15-541-2024>
- [19] Moger, G., Varol, H.A. (2024). Design and implementation of a mobile robot with variable-diameter wheels. *IEEE/ASME Transactions on Mechatronics*, 1-10. <https://doi.org/10.1109/tmech.2024.3457011>
- [20] Arora, H., Das Gupta, P., Kumar, D., Abhishek, Taluja, I., Lachenpa, U.L., Abbas, M. (2024). Design and analysis of a stairs-climbing military bot for efficient and stable movement on various terrains. *International Journal on Interactive Design and Manufacturing (IJIDeM)*, 1-17. <https://doi.org/10.1007/s12008-024-01840-z>
- [21] Phannil, N., Jettanasen, C. (2023). Design and simulation of removable pavement edge climbing electric wheelchair for elderly and disabled users. *International Journal of Control, Automation and Systems*, 21(6): 1910-1925. <https://doi.org/10.1007/s12555-021-0841-2>
- [22] Kim, Y., Son, D., Shin, J., Seo, T. (2023). Optimal design of body profile for stable stair climbing via tri-wheels. *International Journal of Precision Engineering and Manufacturing*, 24(12): 2291-2302. <https://doi.org/10.1007/s12541-023-00887-4>
- [23] Juang, L.H. (2023). Humanoid robot runs up-down stairs using zero-moment with supporting polygons control.

- Multimedia Tools and Applications, 82(9): 13275-13305. <https://doi.org/10.1007/s11042-022-13723-0>
- [24] Zhang, S., Guo, L., Wang, Z. (2020). Stair climbing multifunctional walking robot. *Journal of Physics: Conference Series*, 1570(1): 012032. <https://doi.org/10.1088/1742-6596/1570/1/012032>
- [25] Pappalettera, A., Reina, G., Mantriota, G. (2024). Design and analysis of tracked stair-climbing robot using innovative suspension system. *Robotics*, 13(3): 45. <https://doi.org/10.3390/robotics13030045>
- [26] Shin, J., Son, D., Kim, Y., Seo, T. (2022). Design exploration and comparative analysis of tail shape of tri-wheel-based stair-climbing robotic platform. *Scientific Reports*, 12(1): 19488. <https://doi.org/10.1038/s41598-022-24179-5>
- [27] Navarro, I.J., Martí, J.V., Yepes, V. (2023). Dematel-based completion technique applied for the sustainability assessment of bridges near shore. *International Journal of Computational Methods and Experimental Measurements*, 11(2): 115-122. <https://doi.org/10.18280/ijcmem.110206>
- [28] Keshavarz-Ghorabae, M., Amiri, M., Zavadskas, E.K., Turskis, Z., Antucheviciene, J. (2021). Determination of objective weights using a new method based on the removal effects of criteria (MEREK). *Symmetry*, 13(4): 525. <https://doi.org/10.3390/sym13040525>
- [29] Keshavarz-Ghorabae, M. (2021). Assessment of distribution center locations using a multi-expert subjective-objective decision-making approach. *Scientific Reports*, 11(1): 19461. <https://doi.org/10.1038/s41598-021-98698-y>
- [30] Shanmugasundar, G., Sapkota, G., Čep, R., Kalita, K. (2022). Application of MEREK in multi-criteria selection of optimal spray-painting robot. *Processes*, 10(6): 1172. <https://doi.org/10.3390/pr10061172>
- [31] Silva, N.F., dos Santos, M., Gomes, C.F.S., de Andrade, L.P. (2023). An integrated CRITIC and grey relational analysis approach for investment portfolio selection. *Decision Analytics Journal*, 8: 100285. <https://doi.org/10.1016/j.dajour.2023.100285>
- [32] Sheth, M., Gajjar, K., Jain, A., Shah, V., Patel, H., Chaudhari, R., Vora, J. (2021). Multi-objective optimization of Inconel 718 using combined approach of Taguchi—Grey relational analysis. In *Advances in Mechanical Engineering: Select Proceedings of ICAME 2020*, pp. 229-235. [https://doi.org/10.1007/978-981-15-3639-7\\_27](https://doi.org/10.1007/978-981-15-3639-7_27)
- [33] Chanakyan, C., Sivasankar, S., Meignanamoorthy, M., Alagarsamy, S.V. (2021). Parametric optimization of mechanical properties via FSW on AA5052 using Taguchi based grey relational analysis. *Incas Bulletin*, 13(2): 21-30. <https://doi.org/10.13111/2066-8201.2021.13.2.3>
- [34] Abifarín, J.K. (2021). Taguchi grey relational analysis on the mechanical properties of natural hydroxyapatite: Effect of sintering parameters. *The International Journal of Advanced Manufacturing Technology*, 117(1): 49-57. <https://doi.org/10.1007/s00170-021-07288-9>
- [35] Ikeagwuani, C.C., Agunwamba, J.C., Nwankwo, C.M., Eneh, M. (2021). Additives optimization for expansive soil subgrade modification based on Taguchi grey relational analysis. *International Journal of Pavement Research and Technology*, 14: 138-152. <https://doi.org/10.1007/s42947-020-1119-4>
- [36] Bademlioglu, A.H., Canbolat, A.S., Kaynakli, O. (2020). Multi-objective optimization of parameters affecting organic Rankine cycle performance characteristics with Taguchi-grey relational analysis. *Renewable and Sustainable Energy Reviews*, 117: 109483. <https://doi.org/10.1016/j.rser.2019.109483>
- [37] Awale, A., Inamdar, K. (2020). Multi-objective optimization of high-speed turning parameters for hardened AISI S7 tool steel using grey relational analysis. *Journal of the Brazilian Society of Mechanical Sciences and Engineering*, 42(7): 356. <https://doi.org/10.1007/s40430-020-02433-z>
- [38] Niranján, T., Singaravel, B., Raju, S.S. (2022). Optimization of hole quality parameters using TOPSIS method in drilling of GFRP composite. *Materials Today: Proceedings*, 62: 2109-2114. <https://doi.org/10.1016/j.matpr.2022.03.042>
- [39] Prabhuram, T., Singh, S.P., Durairaj, J.I., Elilraja, D., Das, M.C., Sunderraj, D.A.J. (2022). Optimization of operation parameters in machining of functionally graded metal matrix composite using TOPSIS. *Materials Today: Proceedings*, 62: 429-433. <https://doi.org/10.1016/j.matpr.2022.03.562>
- [40] Singh, G., Kumar, A., Aggarwal, V., Singh, S. (2022). Experimental investigations and optimization of machining performance during turning of EN-31 steel using TOPSIS approach. *Materials Today: Proceedings*, 48: 1089-1094. <https://doi.org/10.1016/j.matpr.2021.07.381>
- [41] Kanagaraju, T., Gowthaman, B., Arunkumar, A., Akash, S. (2022). Optimization of machining parameters in wet and cryogenic machining using TOPSIS approach. *Materials Today: Proceedings*, 62: 1157-1162. <https://doi.org/10.1016/j.matpr.2022.04.346>
- [42] Ranjit, R. (2010). *A Primer on the Taguchi Method*: Society of Manufacturing Engineers.